

# ChemSpaceAL: An Efficient Active Learning Methodology Applied to Protein-Specific Molecular Generation

Gregory W. Kyro<sup>†</sup>, Anton Morgunov<sup>†</sup>, Rafael I. Brent<sup>†</sup>, Victor S. Batista<sup>\*</sup>

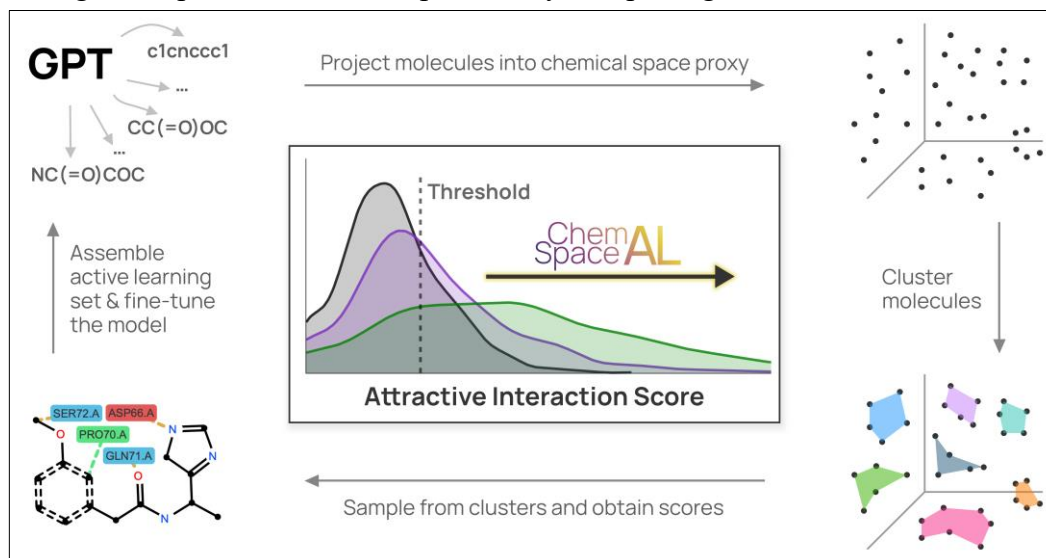
Yale University

<sup>†</sup>equal contribution <sup>\*</sup>corresponding author

{gregory.kyro, anton.morgunov, rafi.brent, victor.batista}@yale.edu

## Abstract

The incredible capabilities of generative artificial intelligence models have inevitably led to their application in the domain of drug discovery. It is therefore of tremendous interest to develop methodologies that enhance the abilities and applicability of these powerful tools. In this work, we present a novel and efficient semi-supervised active learning methodology that allows for the fine-tuning of a generative model with respect to an objective function by strategically operating within a constructed representation of the sample space. In the context of targeted molecular generation, we demonstrate the ability to fine-tune a GPT-based molecular generator with respect to an attractive interaction-based scoring function by strategically operating within a chemical space proxy, thereby maximizing attractive interactions between the generated molecules and a protein target. Importantly, our approach does not require the individual evaluation of all data points that are used for fine-tuning, enabling the incorporation of computationally expensive metrics. We are hopeful that the inherent generality of this methodology ensures that it will remain applicable as this exciting field evolves. To facilitate implementation and reproducibility, we have made all of our software available through the open-source ChemSpaceAL Python package.



# 1. Introduction

The vast majority of pharmaceutical drugs function by targeting a specific protein.<sup>1</sup> A popular method for discovering effective drugs is virtual screening, a computational approach designed to brute-force search a molecular library to identify candidates with high likelihoods of binding to a target protein. The efficacy of virtual screening pipelines is intrinsically tied to the comprehensiveness of the libraries that they screen, and it is therefore beneficial to enrich these libraries with novel drug-like small molecules. While the total number of chemical compounds synthesized to date is approximately  $10^8$ , it is estimated that there are between  $10^{23}$  and  $10^{60}$  theoretically feasible drug-like compounds.<sup>2</sup> Given the challenge of screening on the order of  $10^{23}$  drugs in a computationally feasible manner, it is advantageous to align the design of new molecules to a specific protein of interest, thereby reducing the total search space while simultaneously increasing the probability of generating molecules that will successfully bind.

Artificial intelligence (AI) has recently demonstrated remarkable capabilities in distinct domains, ranging from natural language processing with Generative Pretrained Transformer (GPT)-4 to protein structure prediction with AlphaFold.<sup>3,4</sup> Molecular design methods powered by generative AI have been gaining tremendous attention in recent years, with numerous models based on architectures such as recurrent neural networks (RNNs),<sup>5-27</sup> generative adversarial networks (GANs),<sup>28-40</sup> autoencoders (AEs),<sup>41-61</sup> and transformers.<sup>62-69</sup> RNNs process sequential data by integrating information from current and previous sequence elements, updating their internal state with each iteration. In the case of GANs, a generative component contends with a discriminator trained to distinguish between real and generated data points. This setup enables the generation of new molecules that closely resemble the training distribution with respect to any criteria discernable by the discriminator. AEs, which often make use of RNNs as subcomponents, learn to compress input data into a lower-dimensional latent space and subsequently reconstruct the original input from the latent representation. AEs are able to generate novel molecules by decoding vectors from a regularized latent space. There have also been several AE variants for molecular design, such as training an AE to learn the latent representations of molecules, followed by training a GAN on these latent representations to generate novel latent vectors corresponding to new molecules.<sup>70,71</sup>

The transformer architecture represents one of the most significant advancements in AI, revolutionizing the way models understand and generate sequential data.<sup>72</sup> Central to this innovation is the self-attention mechanism, where an embedding of each token (i.e., sequence element) interacts with embeddings of every other token, yielding weighting factors that establish the strengths of the connections between them. This mechanism enables the model to develop extremely rich internal representations, which have been successfully leveraged for tasks such as language translation,<sup>72</sup> text classification,<sup>73</sup> and next-token prediction.<sup>3</sup> Many groups have investigated the use of transformer units in the field of de novo molecular generation.<sup>62-69</sup>

Many generative models in molecular design, such as those based on RNNs and transformers, utilize sequential data representations. This approach necessitates encoding inherently multi-dimensional molecules as one-dimensional sequences. The predominant method for this conversion is through the simplified molecular-input line-entry system (SMILES), which involves linear representations of molecular structures that can be reverted to their corresponding molecular

connectivity graphs.<sup>74</sup> There is also interest in direct graph-based representations, and several groups have explored molecular generative models based on graph neural networks.<sup>75-82</sup>

In supervised machine learning (ML), the model optimizes its parameters via backpropagation, which involves calculation of the gradient of a loss function with respect to the model's parameters. This gradient indicates the direction for each parameter update, ensuring that each iterative refinement moves the model toward more accurate predictions. Reinforcement learning (RL) has emerged as a prominent alternative across various AI domains, including molecular generation. Unlike supervised learning, RL often employs a reward function that is not differentiable with respect to the model's parameters, preventing the application of backpropagation. Instead, the model in RL is conceptualized as an agent that operates within a defined environment, selecting actions and receiving rewards or penalties based on the outcomes of these actions. In the context of molecular generation, different RL strategies have been implemented using several of the architectures previously mentioned, often involving the evaluation of specific properties of generated molecules. This approach provides the model with quantitative feedback derived from these evaluations, allowing the model to update its parameters accordingly. Research continues into developing and optimizing RL frameworks and strategies for molecular generation beyond the scope of traditional ML architectures.<sup>83-85</sup>

While RL employs quantitative rewards and penalties to update the model's parameters, active learning (AL) refines the model by further training with selectively chosen data points. This refinement typically requires less data, a reduced learning rate, and fewer training epochs compared to the initial pretraining, ensuring that the model retains its broad domain knowledge while narrowing its focus toward a more precise objective. One significant advantage of AL over RL is the potential to utilize unsupervised or semi-supervised learning to curate fine-tuning training sets without performing resource-intensive evaluations of each generated data point. Consequently, a well-constructed sampling algorithm can expose the model to data that span the ideal search space while minimizing computational cost. However, it is crucial to note that if the data chosen for fine-tuning are not judiciously selected, the process can be ineffectual or even detrimental. Hence, the design of the sampling algorithm is paramount in AL methodologies.

Although the application of AL methods to molecular generation is still in its early stages, several noteworthy studies have been published. Ghaemi et al. enhanced an RNN by calculating the Quantitative Estimate of Drug-Likeness (QED)<sup>86</sup> and only retaining molecules with scores that exceed a fixed threshold.<sup>25</sup> In another study, Westermayr et al. refined the outputs of G-SchNet,<sup>89</sup> a model designed for generating three-dimensional molecular structures, by computing a defined property of interest for all generated molecules, and then selecting the molecules with a value greater than one standard deviation above/below the mean for maximization/minimization tasks, respectively.<sup>91</sup> Filella-Merce et al. performed a two-tiered AL strategy using an AE, where the inner loop of their system filters molecules based on criteria such as QED, synthetic accessibility, and similarity to previously retained molecules, and the outer loop operates only on those molecules that pass the inner loop's filters, further refining the AL data based on in silico binding affinity to a specific protein.<sup>53</sup> Notably, a common pattern across these approaches is the calculation of certain properties for every molecule and evaluation of each molecule against set selection criteria. While effective in cases where it is computationally tractable, this approach can be limiting when optimizing over more complex molecular properties that require expensive calculations.

In this work, we present a novel and efficient semi-supervised AL methodology that can align a generative model to a specified objective function without the need to evaluate each data point individually. We demonstrate the efficacy of this method by fine-tuning a molecular generator toward a protein target.

## 2. ChemSpaceAL Methodology and Related Theory

### 2.1 Overview

Our demonstration of the ChemSpaceAL methodology applied to molecular generation proceeds as follows:

- 1) Pretrain our GPT-based model on millions of SMILES strings so that it learns the rules and structure of SMILES notation
- 2) Use the trained model to generate a large number of unique SMILES strings
- 3) Calculate molecular descriptors containing information about molecular topology, physical properties, and presence of functional groups for each generated molecule
- 4) Project the generated SMILES strings into our chemical space proxy
- 5) Use k-means clustering on the generated molecules to group those with similar properties
- 6) Sample a small number of molecules from each cluster and dock each of them to a protein target (e.g., the HNH domain of Cas9)
- 7) Evaluate the top-ranked pose of each protein-ligand complex with a heuristic attractive interaction-based scoring function
- 8) Map the scores back to the original clusters and sample from the clusters proportionately to the cluster scores, combine the sampled molecules with the evaluated molecules whose scores meet or exceed our specified threshold, and include all of them in the AL training set
- 9) Refine our model by fine-tuning it with the AL training set
- \*) Repeat steps (2) – (9) for multiple iterations, guiding the generation toward regions of chemical space that contain molecules with higher scores



particular token only depends on the preceding tokens, while each token in the encoder can attend to all other tokens in the sequence. Our GPT model is constructed as a series of transformer decoder blocks. This approach is appropriate for tasks that require generating novel sequential data such as SMILES strings.

The forward pass of our GPT model begins by dividing each SMILES string into distinct units known as tokens, processing each token with embedding layers, and combining these embeddings to form a vector representation of each token. These embedded vectors are then sequentially passed through a series of transformer decoder blocks, each comprised of a self-attention layer and a feed-forward network, with additional structural elements to enhance learning. The final result is a sequence of vectors, each corresponding to a position in the output SMILES string, where the elements of each vector represent probabilities for each token in the vocabulary. This high-level overview sets the stage for a more detailed discussion of the individual components.

*Embeddings:* Initially, a vocabulary comprising all of the unique tokens in the training data is constructed. For any given SMILES string in the input data, the input tokens undergo three distinct processing methods: token, positional, and type embeddings. The token embedding maps each token in the input sequence to a learnable vector representation, allowing the model to learn an optimal high-dimensional characterization for each token. Similarly, the positional embedding maps each input token to a learnable vector based on its position in the sequence. The type embedding layer uniformly assigns a constant bias to all embeddings of each input sequence. The sum of these three embeddings is passed through a dropout layer, setting 10% of its scalar components to 0. This embedding process transforms the input tokens into a form more suitable for the downstream modeling process.

*Transformer Decoder Stack:* For each token in the input sequence, the resulting embedding is passed to the first transformer decoder block, which begins with layer normalization, a process that adjusts and scales each embedding to have a mean of 0 and a standard deviation of 1. A self-attention mechanism is then applied to the normalized embedding, using learned matrices to linearly transform the embedding into three different vectors known as the query, key, and value vectors:

$$\mathbf{q}_i = \mathbf{W}_q \times \mathbf{e}_i \quad (1)$$

$$\mathbf{k}_i = \mathbf{W}_k \times \mathbf{e}_i \quad (2)$$

$$\mathbf{v}_i = \mathbf{W}_v \times \mathbf{e}_i \quad (3)$$

where  $\mathbf{W}_q$ ,  $\mathbf{W}_k$ , and  $\mathbf{W}_v$  are learned weight matrices that transform each input embedding, represented by  $\mathbf{e}_i$ , into the corresponding query, key, and value vectors. The dot products of the query and each key vector are then scaled according to the dimensionality of the key vectors and passed through a softmax function, transforming them into a probability distribution to serve as attention weights. Finally, the attention scores are used to generate a weighted sum of the value vectors, as shown in the following equation:

$$\mathbf{e}'_i = \mathbf{V} \times \text{softmax} \begin{pmatrix} \frac{\mathbf{q}_i \cdot \mathbf{k}_1}{\sqrt{d_k}} \\ \dots \\ \frac{\mathbf{q}_i \cdot \mathbf{k}_L}{\sqrt{d_k}} \end{pmatrix} \quad (4)$$

Here,  $\mathbf{e}'_i$  represents the output of the attention mechanism at position  $i$  in the sequence,  $\mathbf{V}$  is the value matrix whose  $j^{\text{th}}$  column is the value vector corresponding to the embedding at position  $j$  in the sequence,  $d_k$  denotes the dimensionality of the key vectors, and  $L$  represents the length of the entire sequence. This operation amplifies the information from value vectors corresponding to higher attention weights (i.e., tokens that are more relevant to the current query), while suppressing the information from less relevant value vectors.

In practice, the self-attention mechanism is executed multiple times in parallel through what is known as *multi-head* attention. Each head (i.e., execution) uses its own set of learned linear transformations to generate query, key, and value vectors for all tokens in the sequence for each item in the batch, allowing the model to simultaneously focus on different aspects of the input across the various heads. The outputs from all attention heads are then concatenated and passed through a learned linear transformation to generate the final output of the multi-head attention mechanism.

A residual connection is a shortcut that skips one or more layers and allows the original input to be added directly to the output of those layers. This technique aids in training deeper networks by mitigating the vanishing gradient problem, where the gradients become too small for the network to learn effectively. In the context of GPT models, a residual connection is made by adding the input of the attention mechanism to the output. This sum is then processed using layer normalization, and the transformed embeddings are passed through a feed-forward network using the equation:

$$\mathbf{H} = \text{Dropout}(\mathbf{W}_2 \times \text{GELU}(\mathbf{W}_1 \times \mathbf{E}' + \mathbf{b}_1) + \mathbf{b}_2) \quad (5)$$

where  $\mathbf{H}$  is the output of the feed-forward network,  $\mathbf{E}'$  represents the matrix whose columns are the transformed embeddings, and  $\mathbf{W}_1$  (shape: 1024×256),  $\mathbf{b}_1$  (shape: 1024),  $\mathbf{W}_2$  (shape: 256×1024), and  $\mathbf{b}_2$  (shape: 256) represent the weight matrices and bias vectors of the two linear layers. GELU, or Gaussian Error Linear Unit, is an activation function used to introduce non-linearity into the model. A residual connection is established by summing the input to this feed-forward network with the output.

This entire process is repeated for additional decoder blocks, and the output of the final decoder block is processed with layer normalization. The normalized output is then passed through a learned linear transformation with bias to map the embeddings to the output vocabulary size, and the resulting vectors are processed with softmax to generate the output probabilities at each position in the sequence.

## 2.3 GPT Parameters and Pretraining

Our GPT model is composed of eight transformer decoder blocks, each of which contains eight attention heads, and it embeds inputs into a 256-dimensional space. We pretrain our model using a dataset containing millions of SMILES strings corresponding to valid chemical structures. The objective during pretraining is to train the model to correctly predict the next token in the input sequence given the current and preceding tokens. This task encourages the model to grasp the syntax and structure of SMILES notation as a means of understanding molecular structures. The training process utilizes cross-entropy loss with L2 regularization applied to the linear layers using  $\lambda=0.1$ , and the SophiaG optimizer<sup>87</sup> with  $\beta_1=0.965$ ,  $\beta_2=0.99$  and  $\rho=0.04$ . The learning rate warms up to  $3\times 10^{-4}$  during the first 10% of tokens, then decays to  $3\times 10^{-5}$  using cosine decay. Dropout with a probability of 10% is applied after each feed-forward network except for the output layer to mitigate overfitting, and gradient clipping is used in conjunction with layer normalization to stabilize the optimization process and prevent exploding gradients. All weights are initialized according to a Gaussian distribution with a mean of 0 and a standard deviation of 0.02 except for weights involved in layer normalization, which are initialized to 1, and bias parameters, which are initialized to 0. During pretraining, the model is trained with a batch size of 512 for 30 epochs (*Supporting Information*, Figures S1.1-S1.2).

## 2.4 Dataset Collection and Preprocessing

*Data Collection:* We curate a pretraining set by gathering SMILES strings from multiple datasets:

- **ChemBL 33:** Contains about 2.4 million bioactive molecules with drug-like properties.<sup>88</sup>
- **GuacaMol v1:** Comprises about 1.6 million molecules derived from ChemBL 24 that have been synthesized and tested against biological targets.<sup>89</sup>
- **MOSES:** Encompasses about 1.8 million molecules selected from Zinc 15<sup>90</sup> to maximize internal diversity and suitability for medicinal chemistry.<sup>91</sup>
- **BindingDB (08-2023):** Includes about 1.2 million unique small molecules bound to proteins.<sup>92</sup>

We combine all of the SMILES strings from these sources, filter out the strings that are identified as invalid by the RDKit molecular parser,<sup>93</sup> and remove any duplicate strings to prevent redundancy. The resulting combined dataset contains 5,622,772 unique and valid SMILES strings, with a vocabulary of 196 unique tokens.

*Tokenization Process:* The SMILES strings are tokenized, meaning that they are divided into distinct units, each representing a specific element or feature. Some tokens contain a single character (e.g., “C” for carbon), while others consist of multiple characters (e.g., “Br” for bromine). This tokenization procedure allows the model to capture the syntax of SMILES notation, facilitating the training of the model to recognize patterns and relationships in chemical structures. We find that 106 tokens are represented in the dataset less than 100 times, and an additional 42 tokens occur less than 1,000 times. To reduce the size of our vocabulary (from 196 to 48), we remove all SMILES strings containing at least one token that appears less than 1,000 times in our dataset. Most of the SMILES strings excluded contain rare transition metals or isotopes.



*Data Preprocessing:* The longest SMILES string in the dataset has 1,503 tokens, while 99% of the strings in the dataset have 133 or fewer tokens. We impose a SMILES string length cutoff of 133, and remove any string from the dataset whose length is greater than the cutoff. All remaining SMILES strings are then augmented with a start token “!”, an end-of-sequence token “~”, and are extended to the length of the longest SMILES string in the dataset using a padding token “<”. The resulting pretraining dataset contains 5,539,765 SMILES strings, which are randomly split into training (5,262,776 entries; 95.0%) and validation (276,989 entries; 5.0%) sets.

## 2.5 Constructing Our Chemical Space Proxy

In order to select beneficial molecules to be in our AL training set without having to evaluate each one, we need a way to relate molecules that have been scored to those that have not. To achieve this goal, we construct a proxy for chemical space that is predicated on molecular properties, allowing us to operate within a space where nearby molecules share similar features. We first calculate the full set of molecular descriptors available through RDKit’s CalcMolDescriptors method for each molecule in the pretraining set, encompassing a wide range of molecular properties including structural, topological, geometrical, electronic and thermodynamic characteristics. Among these 209 descriptors, 13 return NaN (not a number) or infinity for at least one SMILES string in the dataset and consequently are discarded, resulting in 196 descriptors (*Supporting Information*, Tables S2.1-S2.3). We then perform Principal Component Analysis (PCA) using these descriptors for all molecules in the pretraining set, and find that 99% of the variance is explained by the first 113 principal components. We use the first 120 principal components to construct a 120-dimensional space, which is used throughout the pipeline as our chemical space proxy. At each iteration, we generate 100,000 unique molecules and project them into this space.

## 2.6 Clustering and Sampling from Chemical Space

After constructing our chemical space proxy and projecting generated molecules into this space, we need a way of grouping molecules that likely have similar scores. We show that position in our constructed representation of chemical space correlates with the objective function (see Results and Discussion), and therefore group data points according to proximity in the chemical space proxy.

*Clustering:* Within our chemical space proxy, we utilize k-means clustering to group molecules that exhibit similar chemical properties, with k set to 100. We employ the k-means++ initialization algorithm, where the first centroid is selected randomly and subsequent centroids are iteratively chosen with a probability proportional to their squared distance from the nearest existing centroid. To mitigate the potential for poor initialization, we perform k-means 100 times, seeking to minimize k-means loss (i.e., the sum of squared distances from each data point to the centroid of its cluster) and variance in cluster sizes. Initially, we sort each of the 100 clusterings by k-means loss, and take the five clusterings with the lowest loss, thereby preserving those with more compact clusters. Of these five, we select the clustering with the lowest variance in cluster size for use in the following stages of the methodology.

*Sampling:* After clustering the generated molecules in our chemical space proxy, we randomly select 10 molecules from each cluster that contains at least 10 molecules, and select all of the molecules from any cluster that contains less than 10 molecules. We then randomly sample from the clusters with more than 10 molecules until we achieve a set of 1,000 molecules.

## 2.7 Docking to a Protein Target and Scoring Protein-Ligand Pairs

Having strategically selected a set of 1,000 molecules, the next steps in our methodology are to dock each molecule to a specific protein target and score the top-ranked pose for each complex. This process allows us to estimate attractive interactions between each selected molecule and the protein target.

*Docking to a Protein Target:* Obtaining a docking pose for each protein-ligand pair is necessary for deriving the protein-ligand interaction fingerprint that we use for scoring. Docking is conducted using the DiffDock software<sup>94</sup> with the HNH domain of Cas9 (PDB ID: 6O56)<sup>95</sup> as our protein target. We select HNH as our protein target because of its moderate size and critical role in the catalytic activity of the CRISPR/Cas9 system. These characteristics make it a computationally manageable candidate that is also relevant to enzymatic biological processes, which are largely influenced by protein-ligand interactions. During the docking inference stage, we utilize 20 inference steps, 10 samples for each complex, and a batch size of 6. It should be noted that since DiffDock is a diffusion generative model, it is inherently stochastic in nature. We select the top-ranked docking pose for each protein-ligand pair, which is subsequently used for scoring.

*Scoring Protein-Ligand Complexes:* We utilize a heuristic scoring function that considers various types of attractive contributions to protein-ligand binding using the *prolif* (Protein-Ligand Interaction Fingerprints) software package<sup>96</sup> and handpicked weights for each interaction type: hydrophobic interactions are scored at 2.5; hydrogen-bond interactions at 3.5; ionic interactions at 7.5; interactions between aromatic rings and cations at 2.5; Van der Waals interactions at 1.0; halogen-bond interactions at 3.0; face-to-face pi-stacking interactions at 3.0; edge-to-face pi-stacking interactions at 1.0; and metallic complexation interactions at 3.0. This is a crude approximation, as the optimal weight of each interaction might vary significantly. Nonetheless, it is suitable as a proof-of-concept and can be replaced with a more precise metric. We score each of the 1,000 selected complexes using this method, thereby determining a score for each molecule to serve as a proxy for its potential to bind the protein target.

## 2.8 Curating the Active Learning Training Set and Fine-Tuning the Model

*Creating the Active Learning Training Set:* After scoring each of the 1,000 protein-ligand pairs, we select  $N$  replicas of each molecule that scores equal to or above a defined threshold of 11, where  $N$  is the smallest integer that achieves a total number of molecules of at least 5,000. We then map all scores back to the original clusters and calculate mean cluster scores, which are converted to sampling fractions with the softmax function. We also consider other methods for converting cluster scores to sampling fractions and report the results in the *Supporting Information* (Figures S3.1-S6.5). We sample  $f_i \times 5,000$  molecules randomly from each cluster to obtain a total of 5,000 molecules, where  $f_i$  is the calculated fraction for sampling from cluster  $i$ . If a given cluster has fewer molecules than would satisfy the calculated fraction, we distribute the surplus among

the other clusters relative to their sampling fractions. We combine these 5,000 molecules with the replicas of molecules that met the scoring threshold to generate a training set for AL of at least 10,000 molecules. This protocol allows us to beneficially incorporate molecules that have not been scored while retaining emphasis on those that have obtained high scores.

*Performing the Active Learning Training:* After compiling the training set to be used for AL, the model is further trained for 10 epochs using a learning rate of  $3 \times 10^{-5}$ , with no warmup and a cosine decay to  $3 \times 10^{-6}$ .

The fine-tuned model is then used to generate 100,000 unique molecules which are subsequently used for another iteration of the pipeline. This iterative approach allows us to locate regions of chemical space corresponding to high-scoring molecules. The process is continued until a satisfactory alignment of the model is achieved.

### 3. Results and Discussion

#### 3.1 Validating Our Pretrained GPT Model

Before presenting the capabilities of our proposed methodology, it is necessary first to demonstrate that our pretrained GPT model is able to generate molecules that are representative of the chemical space spanned by the training set. Visualizing each pretraining set that we use and the corresponding generated molecules projected into our chemical space proxy, we see that our pretrained models are able to generate molecules that sufficiently cover the area spanned by the corresponding pretraining set (Figure 2).

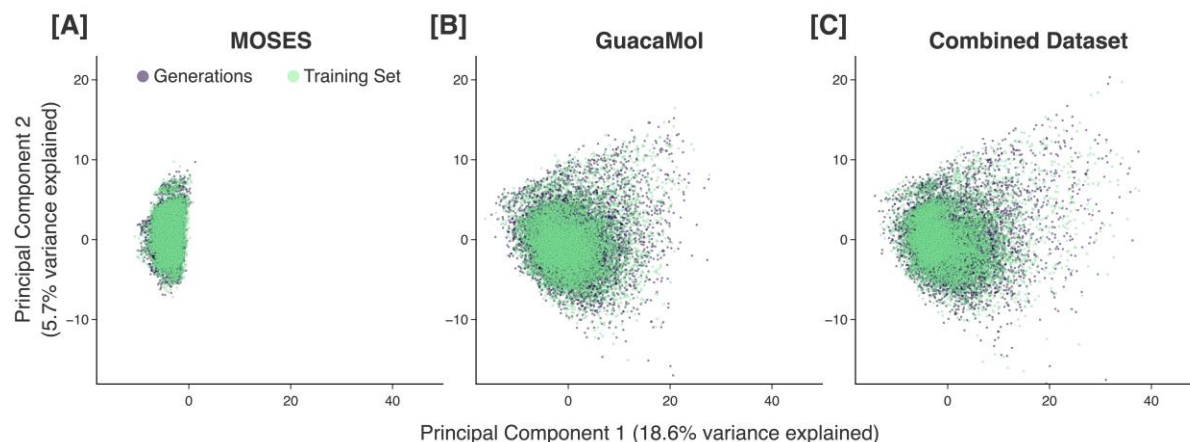


**Figure 2. Different pretraining sets (green) plotted with the molecules generated by the corresponding pretrained model (purple).** Data points are projected onto the first two principal components of our chemical space proxy. Results are shown for the MOSES (A), GuacaMol (B), and combined (C) pretraining sets.

To further substantiate our pretrained GPT model, we show that it is competitive with top-performing models in the field at generating a broad distribution of molecules. Many generative AI models for molecular discovery have been evaluated with the MOSES benchmark.<sup>91</sup> This

benchmark constitutes an important standard for the field, with the objective of assessing models' abilities to generate diverse collections of novel and valid molecules. There are other metrics used in the MOSES benchmark that assess how closely the set of generated molecules resembles the training set, but for more targeted tasks such as protein-binder design, this objective may not be desirable, as the optimal molecules may reside in a small region of chemical space which is not well-represented in the training data. However, it is necessary for our pretrained model to initially generate a wide range of molecules, as this allows our pipeline to begin with a diverse and broad representation of chemical space that can then be refined through AL. For this reason, we evaluate our pretrained model on the complete MOSES benchmark and show that our model performs among the best in the field (*Supporting Information*, Figures S7.1-S7.2), establishing its merit as a starting point for AL. Although we utilize a GPT-based model in this work, we suspect that the model can be successfully substituted as more capable architectures are developed, while still retaining the core advantages of our novel AL methodology.

### 3.2 Substantiating Our Scoring Function and Selection Criterion

We assess the validity of our scoring function with the PDBbind v2020 refined set, which contains 5,316 unique experimentally determined protein-ligand binding complexes with high-quality labels and structures.<sup>97</sup> RDKit fails to interpret 21 of the complexes, and another 112 complexes contain metal atoms that ProLif is not able to process, resulting in a dataset of 5183 complexes. We find that there is a positive Pearson correlation of 0.32 between the scores derived from our heuristic function and the experimentally determined binding affinities (Figure 3A), supporting our scoring function as an approximate yet meaningful proxy for binding ability. Furthermore, we find that 99.6% of the complexes score at least 11, substantiating our choice of threshold value (Figure 3B).

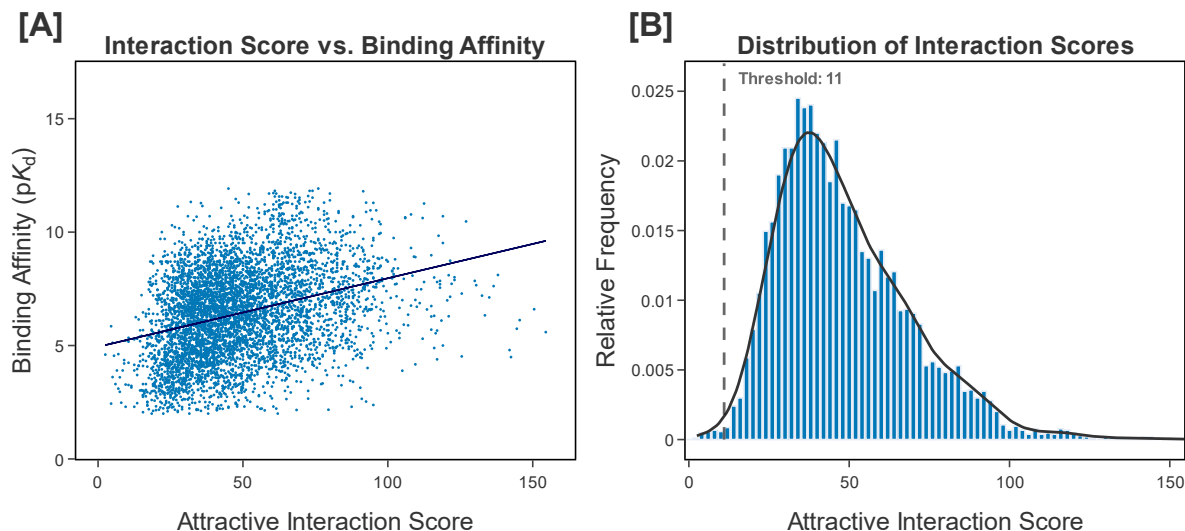


**Figure 3. Evaluation of our attractive interaction-based scoring function with the protein-ligand complexes in the PDBbind v.2020 refined set.** (A) Binding affinity ( $pK_d$ ) plotted as a function of attractive interaction score. There is a corresponding Pearson correlation of 0.32. (B) The relative frequency of different scores. 99.6% of complexes exceed our score threshold of 11.

### 3.3 Performing Naïve Active Learning to Establish a Baseline

In order to establish a control, we perform a naïve version of AL where we generate 100,000 unique molecules, randomly select 1,000 of them, and then dock and score each of the selected molecules. We construct the AL training set from  $N$  replicas of each molecule that scores equal to or above our score threshold, where  $N$  is the smallest integer that achieves a total number of molecules of at least 5,000. We repeat this procedure for five iterations, and observe that the percentage of generated molecules above the score threshold increases from 26.2% to 44.2% (Figure 4A).

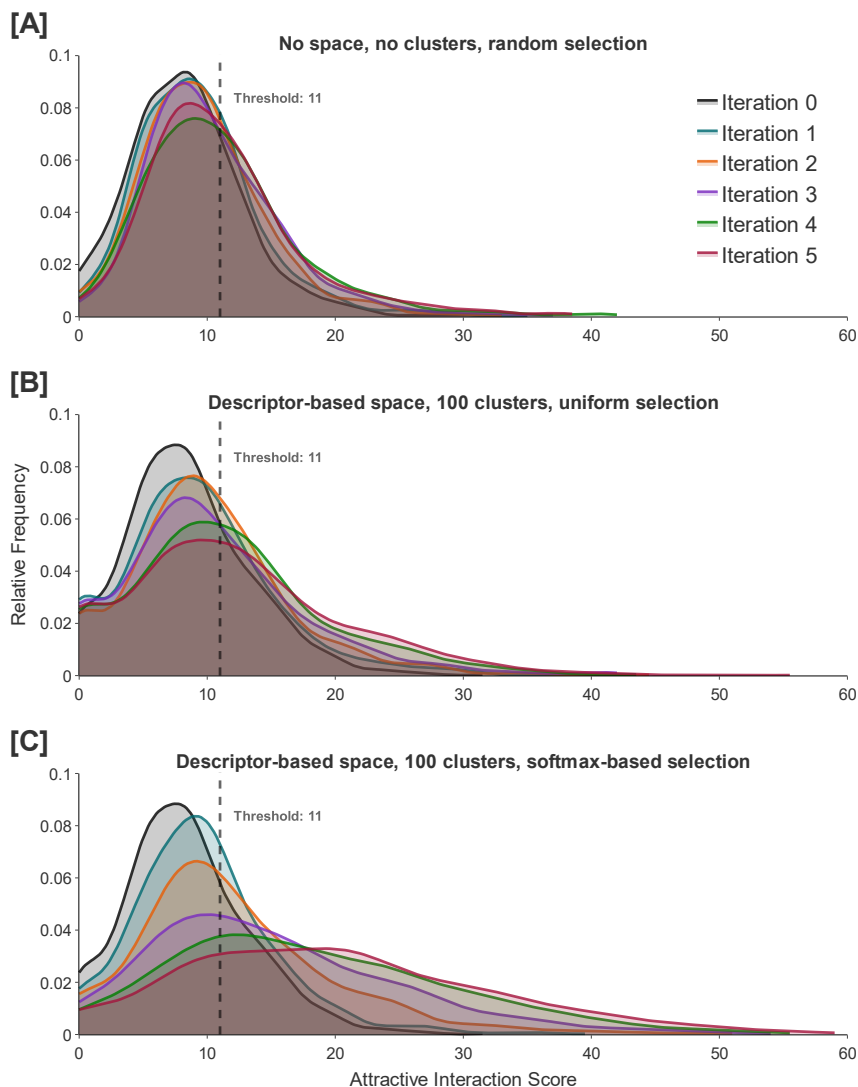


**Figure 4. Attractive interaction scores of scored molecules across five iterations of active learning.** Results for the naïve sampling method are shown in (A), with random selection of molecules and active learning with only those that score equal to or above the score threshold of 11. Results involving only the diffusion effect are shown in (B), with cluster-based sampling where each cluster is assigned a sampling fraction  $f = 0.01$  to generate the active learning set. Results for our proposed active learning methodology are shown in (C). Iteration 0 refers to the pretraining phase, while later iterations refer to the active learning phases.

### 3.4 Validating Our Chemical Space

To improve upon naïve AL, we utilize a clustering method to group molecules with similar properties. In order to achieve this goal, we construct a representation of chemical space that is based on specific molecular characteristics. To locate regions with high scores, a correlation must exist between position in this space and values produced by our scoring function. Visualizing all of the scored molecules from each iteration of our pipeline (6,000 molecules) along the first two principal components of our chemical space proxy, we are able to observe a continuous gradient of scores (Figure 5A), demonstrating the relation between position in our chemical space proxy and values produced by our objective function.

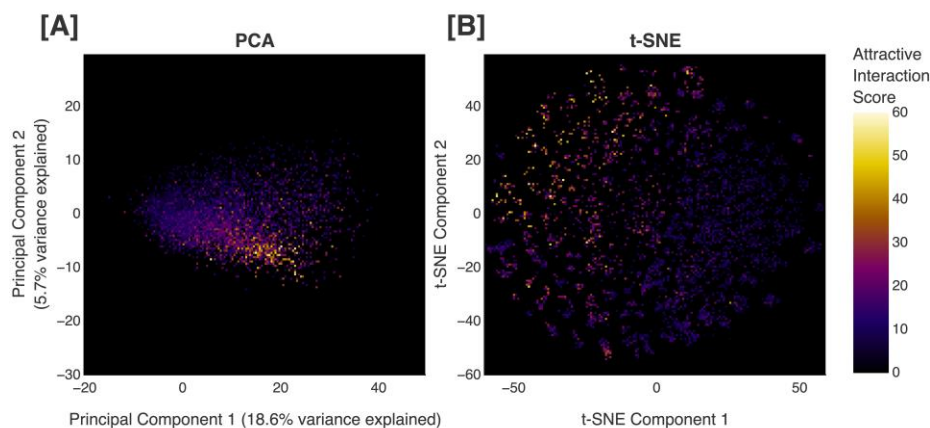


**Figure 5. Visualization of scored molecules in lower-dimensional spaces.** (A) Generated molecules projected along the first two principal components (18.6% and 5.7% of total variance explained, respectively) of our chemical space proxy, and (B) two-dimensional t-distributed stochastic neighbor embedding (t-SNE) plot of the generated molecules. Plots are colored by score obtained with our heuristic attractive interaction-based scoring function, where black/purple corresponds to lower scores and white/yellow corresponds to higher scores.

Moreover, we visualize the scored molecules using t-distributed stochastic neighbor embedding (t-SNE),<sup>98</sup> a dimensionality reduction technique that can capture nonlinear structures often missed by linear methods like PCA. It is worth noting that in this work, we perform t-SNE (perplexity=40, early exaggeration=60) only once to ensure a constant coordinate system for comparison across different AL iterations (full method in *Supporting Information*, Section 8). When the scored molecules are plotted using t-SNE, we see that the regions containing molecules with higher scores are easily identifiable (Figure 5B). These results, in combination with those obtained using PCA, confirm the connection between our approximation to chemical space and our attractive interaction-based scoring function.

### 3.5 Assessing the Diffusion Effect

Because the generated molecules are not evenly distributed in the constructed chemical space, cluster-based sampling introduces a bias in which molecules from less dense regions are sampled more frequently than they are with random selection, leading to a score-independent shift in the

distribution throughout AL iterations. To assess this bias, which we refer to as the *diffusion effect*, we construct AL training sets containing at least 10,000 molecules by selecting molecules with scores equal to or above the defined score threshold (at least 5,000 molecules including replicas) and sampling from each cluster with the same sampling fraction  $f = 0.01$  (5,000 molecules). Notably, the magnitude of the shift in the score distribution is slightly larger than that achieved via random selection (Figure 4B). Specifically, the percentage of generated molecules equal to or greater than our score threshold increases from 28.1% to 51.1% after five iterations of AL.

### 3.6 Evaluating the Capabilities of the ChemSpaceAL Methodology

In contrast to our protocol for assessing the diffusion effect, our complete pipeline involves sampling from clusters according to fractions obtained by applying the softmax function to the mean cluster scores. We observe that the percentage of generated molecules with scores equal to or greater than the score threshold is increased from 28.1% to 76.0% after five iterations of AL, nearly a three-fold enhancement (Figure 4C). More detailed metrics regarding the continuous improvement of the distribution of generated molecules are shown in Table 1.

**Table 1. Statistics regarding the distribution of generated molecules across our complete active learning pipeline.**

Iteration	Percent > 11	Q1	Q2	Mean	Q3	Max
0	28.1%	5.5	8.0	8.0	11.5	31.5
1	37.0%	6.0	9.0	9.8	12.5	39.5
2	49.7%	7.5	10.5	12.2	16.0	51.0
3	62.6%	8.0	13.5	15.1	20.6	54.0
4	72.9%	10.0	16.5	18.2	25.0	55.5
5	76.0%	11.0	19.0	20.1	27.6	59.0

<sup>a</sup> The percentage of generated molecules with attractive interaction scores equal to or above our score threshold is shown (Percent > 11), as well as the score at the first quartile (Q1), second quartile (Q2), mean, third quartile (Q3), and maximum of the distribution.

<sup>b</sup> Iteration 0 refers to the pretraining phase, while later iterations refer to the active learning phases.

After each AL iteration, the percentage of generated molecules with scores above the score threshold, the mean score, the scores at the first, second, and third quartiles, as well as the maximum score all increase, indicating that the broad population of generated molecules is enhanced throughout our methodology. Since 99.6% of protein-ligand complexes in the PDBbind v2020 refined set exhibit scores equal to or above the score threshold (Figure 3B), this threshold empirically constitutes a minimal requirement for binding. Therefore, almost 72% of the molecules initially generated by the pretrained model have a near-zero probability of binding, while this metric plummets to 24% after employing our methodology, indicating a vast improvement of the resulting library.

### 3.7 Further Analyzing Our Sampling Approach

If our sampling approach were insufficient at differentiating between distinct regions within the generated distribution, we would expect to create AL training sets that were highly similar to the generated distribution at the same iteration. Figure 6A-B and Figure 7A-B demonstrate that this is not the case, showing that certain subregions are amplified or suppressed at each iteration. Furthermore, in Figure 6C-D and Figure 7C-D, it is clear that both the generated and AL sets evolve significantly relative to the generations from iteration 0. Visualizing the evolution of the generated and AL sets, we see that our methodology shifts the distributions continuously and in a constant direction.

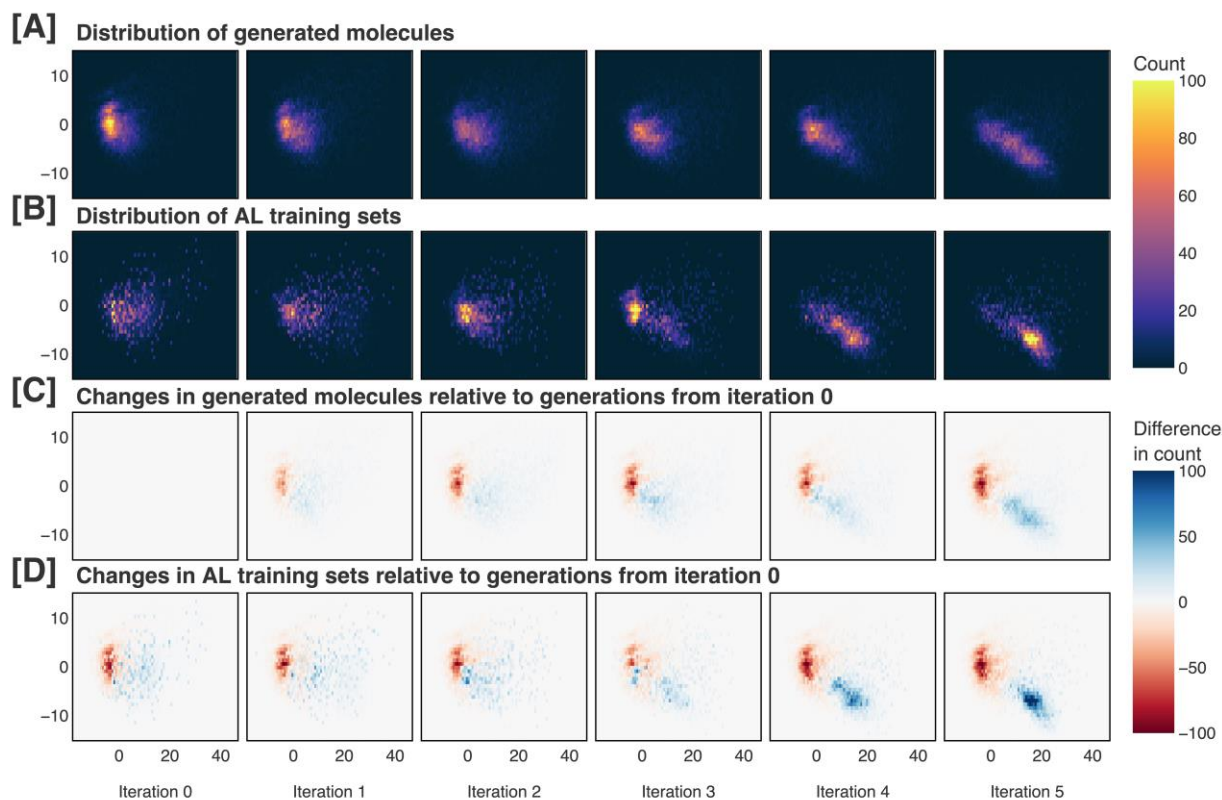


**Figure 6. Generated molecules and active learning training sets across each iteration of our pipeline, visualized along the first two principal components of our chemical space proxy.** The generated molecules and active learning training sets are shown in (A) and (B), respectively. Changes in the generated molecules and active learning training sets relative to the molecules generated at iteration 0 are shown in (C) and (D), respectively. Iteration 0 refers to the pretraining phase, while later iterations refer to the active learning phases.



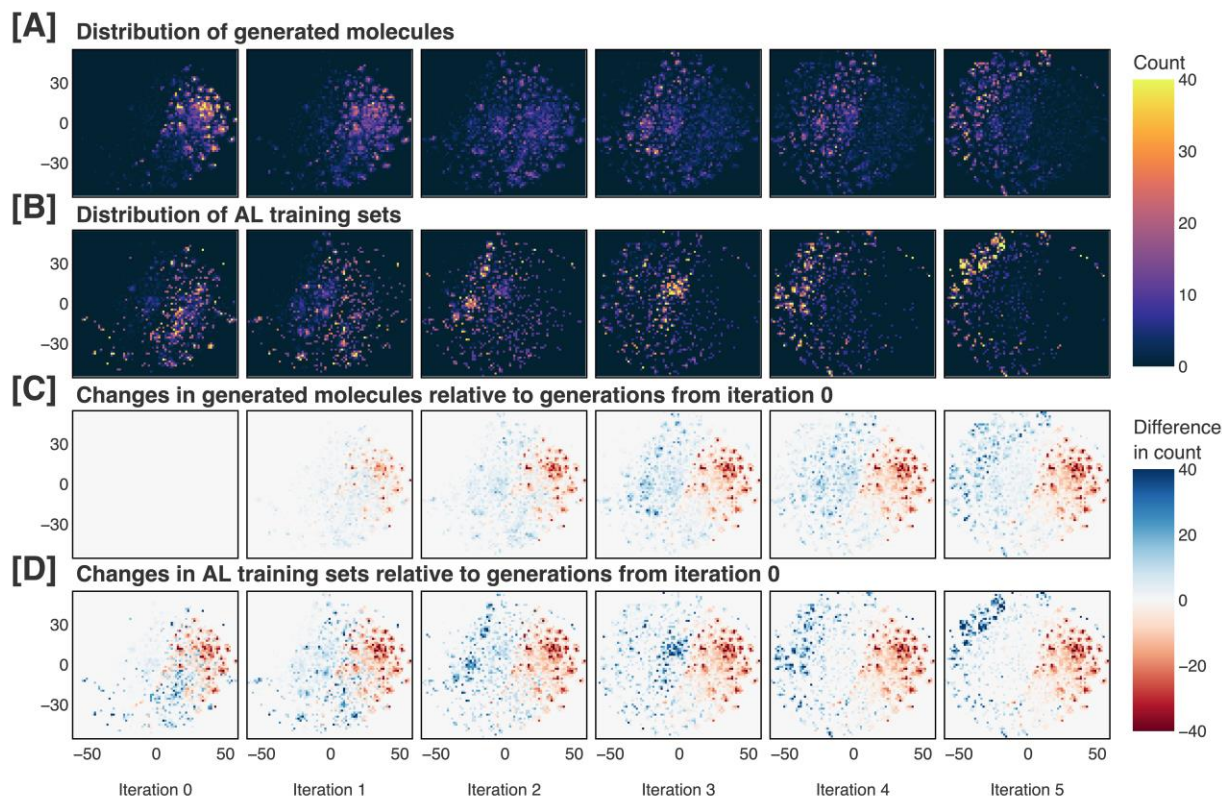


**Figure 7. Generated molecules and active learning training sets across each iteration of our pipeline, visualized in two dimensions after performing t-distributed stochastic neighbor embedding (t-SNE).** The generated molecules and active learning training sets are shown in (A) and (B), respectively. Changes in the generated molecules and active learning training sets relative to the molecules generated at iteration 0 are shown in (C) and (D), respectively. Iteration 0 refers to the pretraining phase, while later iterations refer to the active learning phases.

## 4. Summary

We have developed a novel AL methodology that can efficiently improve the outputs of a generative model with respect to an objective function by strategically operating within a constructed sample space. We demonstrate the capabilities of this methodology in the context of targeted molecular generation by fine-tuning a GPT model to produce molecules that exhibit higher attractive interaction scores with the HNH domain of Cas9. In contrast to previous AL methods for molecular generation, our approach does not require scoring each data point that is included in the AL training set, allowing for the incorporation of more computationally expensive metrics such as those requiring protein-ligand docking poses.

## 5. Future Outlook

We envision that the interchangeability of the generative model, constructed sample space, and scoring function renders our methodology adaptable to future innovations. For instance, the GPT model could be replaced by a more capable architecture as soon as one is developed. In addition, rather than constructing a sample space from molecular descriptors, any quantifiable features that are related to the defined objective function can be used. In the context of molecular generation, the list of descriptors used to construct our chemical space proxy could be substituted as better molecular descriptors are developed. Moreover, the scoring function that we use can be replaced by a more computationally expensive metric such as a molecular mechanics-based scoring function to achieve higher precision. The efficiency and generality of our approach facilitate the applicability and utility of the ChemSpaceAL methodology both at present and as the state of the field inevitably improves.

### **Data and Software Availability**

All of our software is available as open source at <https://github.com/gregory-kyro/ChemSpaceAL/>. Additionally, the ChemSpaceAL Python package is available via PyPI at <https://pypi.org/project/ChemSpaceAL/>.

### **Author Information**

**Corresponding Author:** Victor S. Batista

Phone: (203) 432-6672

Email: [victor.batista@yale.edu](mailto:victor.batista@yale.edu)

**Present Address:** Department of Chemistry, Yale University, New Haven, Connecticut 06511-8499

### **Author Contributions**

GWK, AM, RIB designed research; GWK, AM, RIB developed software; GWK, AM, RIB published the Python package; GWK, AM, RIB performed research; GWK, AM, RIB, VSB analyzed data; and GWK, AM, RIB wrote the paper. All authors have given approval to the final version of the manuscript.

‡GWK, AM, RIB contributed to this work equally

## **Funding Sources**

National Institutes of Health: Grants R01GM136815

National Science Foundation: Grant DGE-2139841

## **Acknowledgments**

We acknowledge financial support from the National Institutes of Health under Grant R01GM136815, as well as from the National Science Foundation under Grant DGE-2139841. VSB also acknowledges high-performance computer time from the National Energy Research Scientific Computing Center and from the Yale University Faculty of Arts and Sciences High Performance Computing Center.

## **Abbreviations**

AI, artificial intelligence; GPT, generative pretrained transformer; RNNs, recurrent neural networks; GANs, generative adversarial networks; AEs, autoencoders; SMILES, simplified molecular-input line-entry system; ML, machine learning; RL, reinforcement learning; AL, active learning; QED, quantitative estimate of drug-likeness; NaN, not a number; PCA, principal component analysis; t-SNE, t-distributed stochastic neighbor embedding.

## **Supporting Information**

The Supporting Information contains figures and tables regarding the following aspects: Training our generative model; Construction of the chemical space proxy from RDKit descriptors; Alternative methods for converting mean cluster scores to sampling fractions; Evolution of the distribution of attractive interaction scores for different conversion methods; Evolution of the distribution of the number of attractive interactions for different conversion methods; Evolution of the distribution of cluster-average attractive interaction scores for different conversion methods; Performance on the MOSES benchmark; Implementation of t-distributed stochastic neighbor embedding; Vocabulary composition of the combined dataset; Choosing the number of clusters to use for k-means; Additional evaluation of generations across active learning iterations.

# Supporting Information

## List of Figures and Tables

### Section 1: Training our generative model

- **1.1:** Training loss, validation loss and learning rate during the 30 epochs of pretraining of our model on the combined dataset.
- **1.2:** Training step losses (evaluated after each batch) during 5 rounds of active learning (10 epochs each) with different conversion methods.

### Section 2: Construction of the chemical space proxy from RDKit descriptors

- **2.1:** List of RDKit descriptors used for the construction of the chemical space proxy.
- **2.2:** List of RDKit descriptors excluded prior to performing Principal Component Analysis.
- **2.3:** Cumulative fraction of variance explained by the first  $N$  principal components.

### Section 3: Alternative methods for converting mean cluster scores to sampling fractions

- **3.1:** Distribution of sampling fractions obtained with different conversion methods applied to cluster scores obtained from generations of the pretrained model.

### Section 4: Evolution of the distribution of attractive interaction scores for different conversion methods

- **4.1:** Attractive interaction scores for molecules generated by the pretrained model (iteration 0) and by the model after each of the five iterations of active learning where, prior to sampling for docking, molecules in the chemical space are grouped into 100 clusters, and cluster scores are converted into sampling fractions using the *linear* method.
- **4.2:** Attractive interaction scores for molecules generated by the pretrained model (iteration 0) and by the model across each of the five iterations of active learning where, prior to sampling for docking, molecules in the chemical space are grouped into 100 clusters, and cluster scores are converted into sampling fractions using the *softdiv* method.
- **4.3:** Statistics of the distribution of attractive interaction scores, when molecules are selected *randomly* (naïve active learning), with no clustering.
- **4.4:** Statistics of the distribution of attractive interaction scores, when molecules are clustered into 100 groups and cluster scores are sampled *uniformly*.
- **4.5:** Statistics of the distribution of attractive interaction scores, when molecules are clustered into 100 groups and cluster scores are converted into sampling fractions using the *linear* method.
- **4.6:** Statistics of the distribution of attractive interaction scores, when molecules are clustered into 100 groups and cluster scores are converted into sampling fractions using the *softdiv* method.

**Section 5:** Evolution of the distribution of the number of attractive interactions for different conversion methods

- **5.1:** Counts of interactions of each type for 1000 scored molecules generated by the pretrained model (iteration 0) and by the model after each of the five rounds of naïve active learning with *random* sampling.
- **5.2:** Counts of interactions of each type for 1000 molecules generated by the pretrained model (iteration 0) and by the model after each of the five rounds of active learning with clustering into 100 groups and *uniform* selection from each cluster.
- **5.3:** Counts of interactions of each type for 1000 scored molecules generated by the pretrained model (iteration 0) and by the model after each of the five rounds of active learning with clustering into 100 groups and conversion of cluster scores into sampling fractions using the *linear* method.
- **5.4:** Counts of interactions of each type for 1000 scored molecules generated by the pretrained model (iteration 0) and by the model after each of the five rounds of active learning with clustering into 100 groups and conversion of cluster scores into sampling fractions using the *softdiv* method.
- **5.5:** Counts of interactions of each type for 1000 molecules generated by the pretrained model (iteration 0) and by the model after each of the five rounds of active learning with clustering into 100 groups and conversion of cluster scores into sampling fractions using the *softsub* method.

**Section 6:** Evolution of the distribution of cluster-average attractive interaction scores for different conversion methods

- **6.1:** Cluster scores (obtained as an average of attractive interaction scores for molecules in the cluster) for molecules generated by the pretrained model (iteration 0) and by the model after each of the five iterations of active learning where, prior to sampling for docking, molecules in the chemical space are grouped into 100 clusters, and molecules are sampled from each cluster *uniformly*.
- **6.2:** Cluster scores (obtained as an average of attractive interaction scores for molecules in the cluster) for molecules generated by the pretrained model (iteration 0) and by the model after each of the five iterations of active learning where, prior to sampling for docking, molecules in the chemical space are grouped into 100 clusters, and molecules are sampled from each cluster using the *linear* method.
- **6.3:** Cluster scores (obtained as an average of attractive interaction scores for molecules in the cluster) for molecules generated by the pretrained model (iteration 0) and by the model after each of the five iterations of active learning where, prior to sampling for docking, molecules in the chemical space are grouped into 100 clusters, and molecules are sampled from each cluster using the *softdiv* method.
- **6.4:** Cluster scores (obtained as an average of attractive interaction scores for molecules in the cluster) for molecules generated by the pretrained model (iteration 0) and by the model after each of the five iterations of active learning where, prior to sampling for docking, molecules in the chemical space are grouped into 100 clusters, and molecules are sampled from each cluster using the *softsub* method.
- **6.5:** Cluster scores (obtained as an average of attractive interaction scores for molecules in the cluster) for molecules generated by the pretrained model (iteration 0) and by the model after each of the five iterations of active learning where, prior to sampling for docking,

molecules in the chemical space are grouped into 10 clusters, and molecules are sampled from each cluster using the *softsub* method.

### **Section 7:** Performance on the MOSES benchmark

- **7.1:** Primary results of our pretrained model on the MOSES benchmark compared to top-performing models in the field.
- **7.2:** Additional results of our pretrained model on the MOSES benchmark compared to top-performing models in the field.

### **Section 8:** Details on the execution of t-distributed stochastic neighbor embedding (t-SNE)

### **Section 9:** Vocabulary composition of the combined dataset

- **9.1:** List of unique tokens that occur in the raw combined dataset less than 1,000 times.
- **9.2:** List of unique tokens in the processed combined dataset.

### **Section 10:** Choosing the number of clusters to use for k-means

- **10.1:** Attractive interaction scores for molecules generated by the pretrained model (iteration 0) and by the model after each of the five iterations of active learning where, prior to sampling for docking, molecules in the chemical space are grouped into 10 clusters, and cluster scores are converted into sampling fractions using the *softsub* approach.
- **10.2:** Attractive interaction scores for molecules generated by the pretrained model (iteration 0) and by the model after each of the five iterations of active learning where, prior to sampling for docking, molecules in the chemical space are grouped into 100 clusters, and cluster scores are converted into sampling fractions using the *softsub* approach.
- **10.3:** Statistics of the distribution of attractive interaction scores, when molecules are clustered into 10 groups and cluster scores are converted into sampling fractions using the *softsub* method.
- **10.4:** Statistics of the distribution of attractive interaction scores, when molecules are clustered into 100 groups and cluster scores are converted into sampling fractions using the *softsub* method.

### **Section 11:** Additional evaluation of generations across active learning iterations

- **11.1.** Percentage of molecules generated by our model that are valid, unique, or novel after pretraining (iteration 0) and five rounds of active learning.
- **11.2.** Memorization of training sets by our model over five rounds of naïve active learning with random selection.
- **11.3.** Memorization of training sets by our model over five rounds of active learning with 100 clusters and *uniform* selection.
- **11.4.** Memorization of training sets by our model over five rounds of active learning with 100 clusters and *linear* selection.
- **11.5.** Memorization of training sets by our model over five rounds of active learning with 100 clusters and *softdiv* selection.
- **11.6.** Memorization of training sets by our model over five rounds of active learning with 100 clusters and *softsub* selection.

## Section 1: Training our generative model

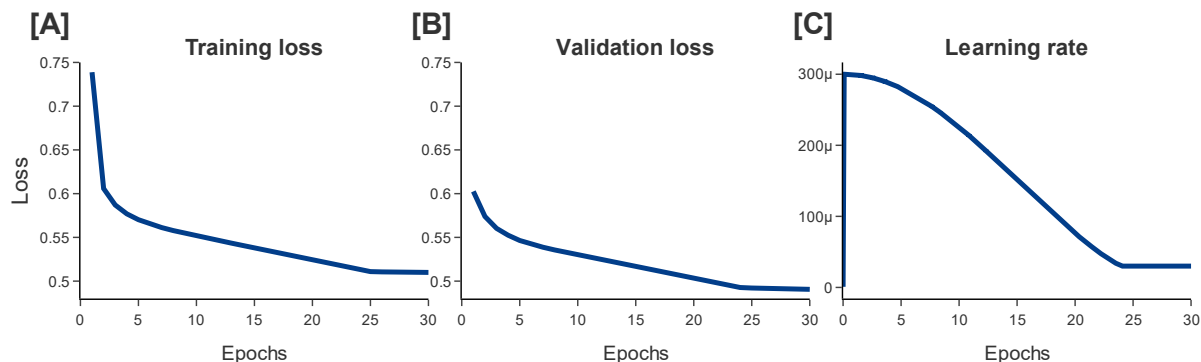


**Figure S1.1.** Training loss (A), validation loss (B), and learning rate (C) during the 30 epochs of pretraining of our model on the combined dataset.

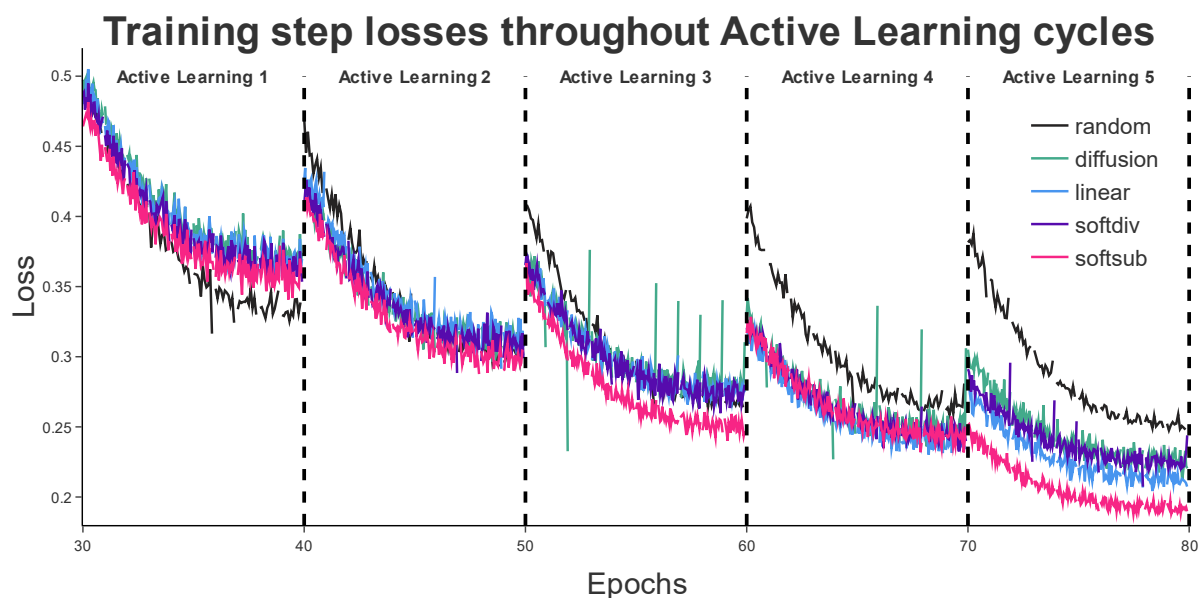


**Figure S1.2.** Training step losses (evaluated after each batch) during 5 rounds of active learning (10 epochs each) with different conversion methods.

## Section 2: Construction of the chemical space proxy from RDKit descriptors

**Table S2.1.** List of RDKit descriptors used for the construction of the chemical space proxy.

- AvgIpc	- MinAbsEState	- PEOE_VSA3
- BalabanJ	Index	- PEOE_VSA4
- BertzCT	- MinEStateIndex	- PEOE_VSA5
- Chi0	- MolLogP	- PEOE_VSA6
- Chi0n	- MolMR	- PEOE_VSA7
- Chi0v	- MolWt	- PEOE_VSA8
- Chi1	- NHOHCount	- PEOE_VSA9
- Chi1n	- NOCount	- RingCount
- Chi1v	- NumAliphatic	- SMR_VSA1
- Chi2n	Carbocycles	- SMR_VSA10
- Chi2v	- NumAliphatic	- SMR_VSA2
- Chi3n	Heterocycles	- SMR_VSA3
- Chi3v	- NumAliphatic	- SMR_VSA4
- Chi4n	Rings	- SMR_VSA5
- Chi4v	- NumAromatic	- SMR_VSA6
- EState_VSA1	Carbocycles	- SMR_VSA7
- EState_VSA10	- NumAromatic	- SMR_VSA8
- EState_VSA11	Heterocycles	- SMR_VSA9
- EState_VSA2	- NumAromatic	- SlogP_VSA1
- EState_VSA3	Rings	- SlogP_VSA10
- EState_VSA4	- NumHAcceptors	- SlogP_VSA11
- EState_VSA5	- NumHDonors	- SlogP_VSA12
- EState_VSA6	- NumHeteroatoms	- SlogP_VSA2
- EState_VSA7	- NumRadical	- SlogP_VSA3
- EState_VSA8	Electrons	- SlogP_VSA4
- EState_VSA9	- NumRotatable	- SlogP_VSA5
- ExactMolWt	Bonds	- SlogP_VSA6
- FpDensityMorgan1	- NumSaturated	- SlogP_VSA7
- FpDensityMorgan2	Carbocycles	- SlogP_VSA8
- FpDensityMorgan3	- NumSaturated	- SlogP_VSA9
- FractionCSP3	Heterocycles	- TPSA
- HallKierAlpha	- NumSaturated	- VSA_EState1
- HeavyAtomCount	Rings	- VSA_EState10
- HeavyAtomMolWt	- NumValence	- VSA_EState2
- Kappa1	Electrons	- VSA_EState3
- Kappa2	- PEOE_VSA1	- VSA_EState4
- Kappa3	- PEOE_VSA10	- VSA_EState5
- LabuteASA	- PEOE_VSA11	- VSA_EState6
- MaxAbsEState	- PEOE_VSA12	- VSA_EState7
Index	- PEOE_VSA13	- VSA_EState8
- MaxEStateIndex	- PEOE_VSA14	- VSA_EState9
	- PEOE_VSA2	- fr_Al_COO



- fr\_Al\_OH
- fr\_Al\_OH\_noTert
- fr\_ArN
- fr\_Ar\_COO
- fr\_Ar\_N
- fr\_Ar\_NH
- fr\_Ar\_OH
- fr\_COO
- fr\_COO2
- fr\_C\_O
- fr\_C\_O\_noCOO
- fr\_C\_S
- fr\_HOCCN
- fr\_Imine
- fr\_NH0
- fr\_NH1
- fr\_NH2
- fr\_N\_O
- fr\_Ndealkylation1
- fr\_Ndealkylation2
- fr\_Nhpyrrole
- fr\_SH
- fr\_aldehyde
- fr\_alkyl\_carbamate
- fr\_alkyl\_halide
- fr\_allylic\_oxid
- fr\_amide
- fr\_amidine
- fr\_aniline
- fr\_aryl\_methyl
- fr\_azide
- fr\_azo
- fr\_barbitur
- fr\_benzene
- fr\_benzodiazepine
- fr\_bicyclic
- fr\_diazo
- fr\_dihydropyridine
- fr\_epoxide
- fr\_ester
- fr\_ether
- fr\_furan
- fr\_guanido
- fr\_halogen
- fr\_hdrzine
- fr\_hdrzone
- fr\_imidazole
- fr\_imide
- fr\_isocyan
- fr\_isothiocyan
- fr\_ketone
- fr\_ketone\_Topliiss
- fr\_lactam
- fr\_lactone
- fr\_methoxy
- fr\_morpholine
- fr\_nitrile
- fr\_nitro
- fr\_nitro\_ arom
- fr\_nitro\_ arom\_ nonortho
- fr\_nitroso
- fr\_oxazole
- fr\_oxime
- fr\_para\_ hydroxylation
- fr\_phenol
- fr\_phenol\_ noOrthoHbond
- fr\_phos\_acid
- fr\_phos\_ester
- fr\_piperdine
- fr\_piperzine
- fr\_priamide
- fr\_prisulfonamd
- fr\_pyridine
- fr\_quatN
- fr\_sulfide
- fr\_sulfonamd
- fr\_sulfone
- fr\_term\_acetylene
- fr\_tetrazole
- fr\_thiazole
- fr\_thiocyan
- fr\_thiophene
- fr\_unbrch\_alkane
- fr\_urea
- qed

**Table S2.2.** List of RDKit descriptors excluded prior to performing Principal Component Analysis.

- BCUT2D\_CHGHI
- BCUT2D\_CHGLO
- BCUT2D\_LOGPHI
- BCUT2D\_LOGPLOW
- BCUT2D\_MRHI
- BCUT2D\_MRLOW
- BCUT2D\_MWHI
- BCUT2D\_MWLOW
- Ipc
- MaxAbsPartialCharge
- MaxPartialCharge
- MinAbsPartialCharge
- MinPartialCharge

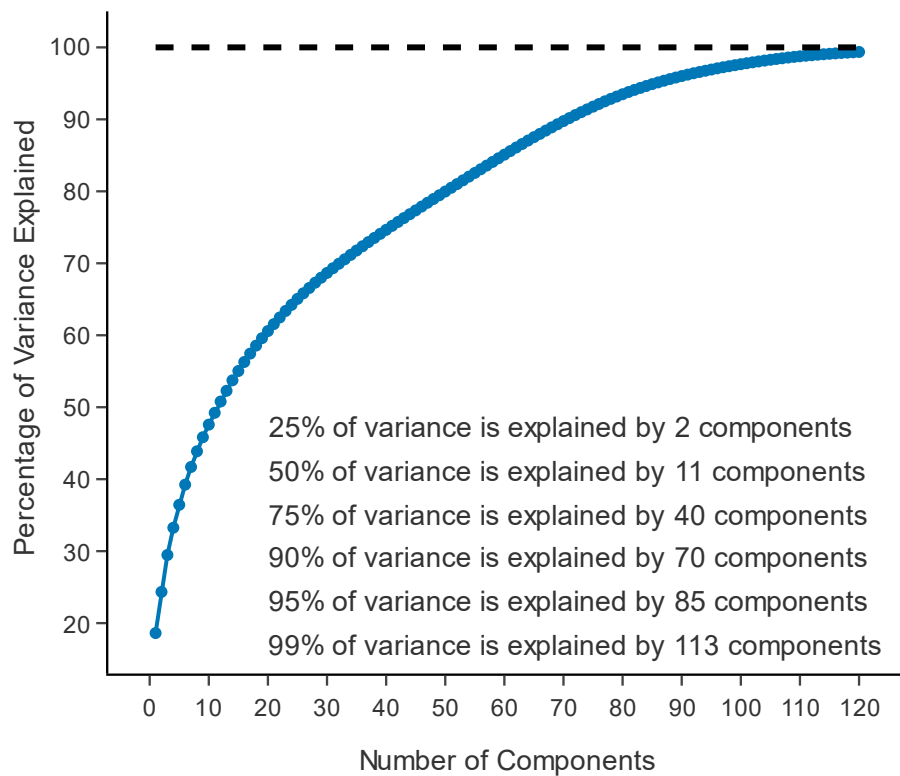


**Figure S2.3.** Cumulative fraction of variance explained by the first  $N$  principal components. Our chemical space proxy (i.e., the first 120 principal components) explains 99.3% of the variance in the hyperspace of 196 RDKit descriptors.

### Section 3: Alternative methods for converting mean cluster scores to sampling fractions

Prior to constructing the active learning training set, we need to convert the attractive interaction scores  $s_i$  obtained by using the *prolif* software on docked molecules into sampling fractions  $f_i$ , which will be used to calculate the number of molecules that we need to sample from each cluster. A simple way to do that is to normalize the sum of all scores to unity:

$$f_i^{\text{linear}}(s_i) = \frac{s_i}{\sum_i s_i}$$

We call this approach *linear* conversion. Because one could interpret sampling fractions as effective probabilities of sampling from a given cluster, it is natural to consider the use of a softmax function:

$$f_i^{\text{softmax}}(s_i) = \frac{e^{s_i}}{\sum_i e^{s_i}}$$

which, for computational stability purposes, is often implemented with the maximum value among a set of arguments subtracted from each individual argument. To contrast with a modification of a softmax function introduced later, we refer to this as *softsub* conversion. In the main text of our paper, we implement the *softsub* approach and refer to it as *softmax* because this is the common implementation of the softmax function.

$$f_i^{\text{softsub}}(s_i) = \frac{e^{s_i - s_{\max}}}{\sum_i e^{s_i - s_{\max}}}$$

For a pretrained model, cluster scores range from 0 to 16. Because exponential functions increase rapidly, the *softsub* approach will effectively favor the 1-5 clusters with largest scores. We conjecture that a smoother function may lead to better model behavior during active learning, and implement a *softdiv* conversion approach, in which, instead of subtracting the maximum cluster score, we divide by it:

$$f_i^{\text{softdiv}}(s_i) = \frac{e^{s_i/s_{\max}}}{\sum_i e^{s_i/s_{\max}}}$$

Empirically, this approach leads even to a narrower distribution of sampling fractions than that obtained with the *linear* conversion approach. We introduce a hyperparameter  $divf \in (0,1]$  by which we multiply the  $s_{\max}$  value prior to dividing by it:

$$f_i^{\text{softdivf}}(s_i) = \frac{e^{\frac{s_i}{divf \times s_{\max}}}}{\sum_i e^{\frac{s_i}{divf \times s_{\max}}}}$$

By visualizing the distribution of *softdiv* values with different values of the hyperparameter (Figure S4.1), we pick  $divf = 0.25$ , as it maximizes the spread in sampling fractions. In what follows, the *softdiv* conversion will refer to *softdiv* with  $divf = 0.25$ .

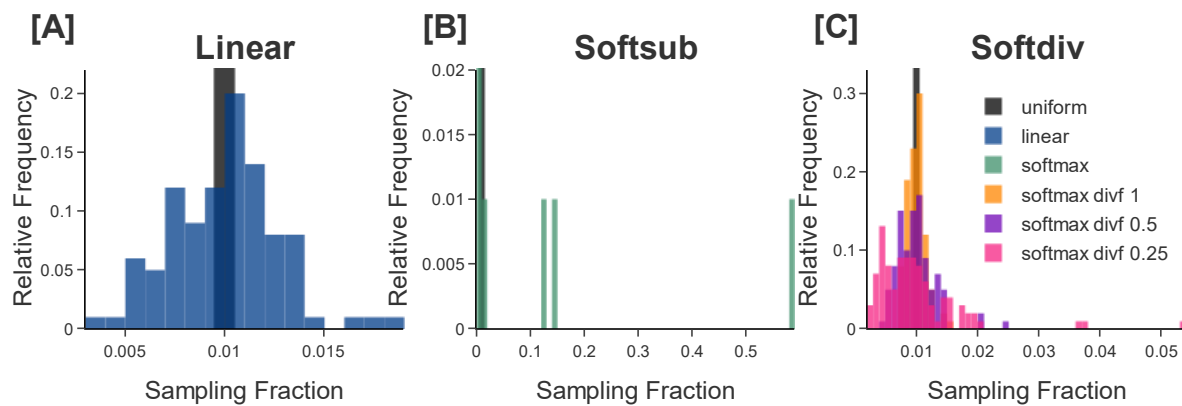


**Figure S3.1.** Distribution of sampling fractions obtained with different conversion approaches applied to cluster scores obtained from generations of the pretrained model. A bar corresponding to sampling the same number of molecules from each cluster (i.e., uniform sampling) is shown in black.

**Section 4:** Evolution of the distribution of attractive interaction scores for different conversion methods

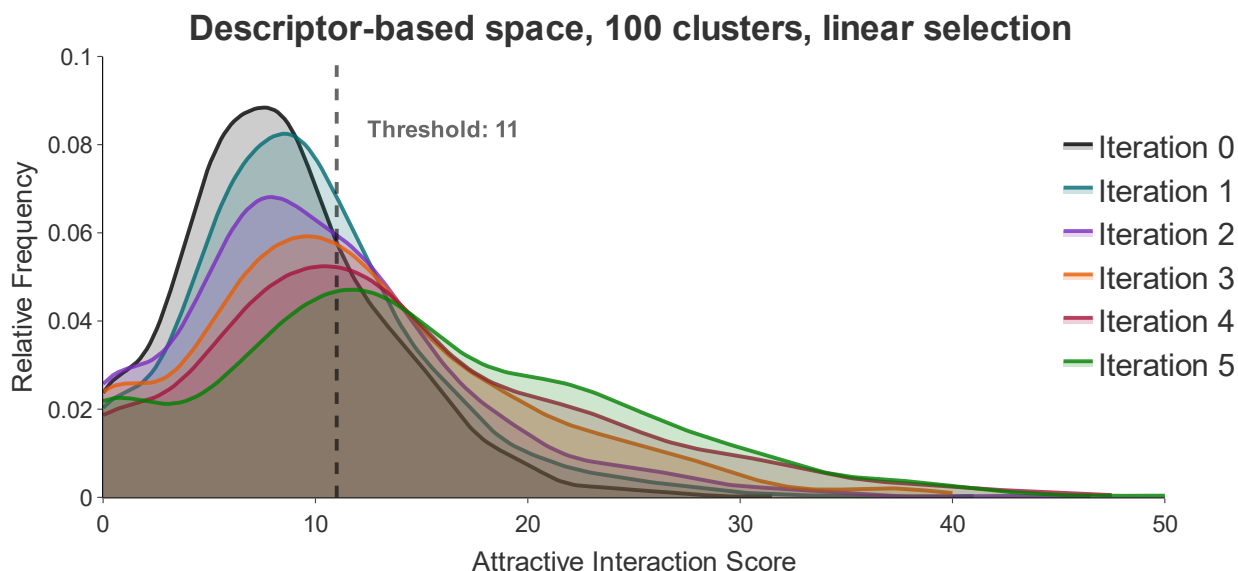


**Figure S4.1.** Attractive interaction scores for molecules generated by the pretrained model (iteration 0) and by the model after each of the five iterations of active learning where, prior to sampling for docking, molecules in the chemical space are grouped into 100 clusters, and cluster scores are converted into sampling fractions using the *linear* approach.

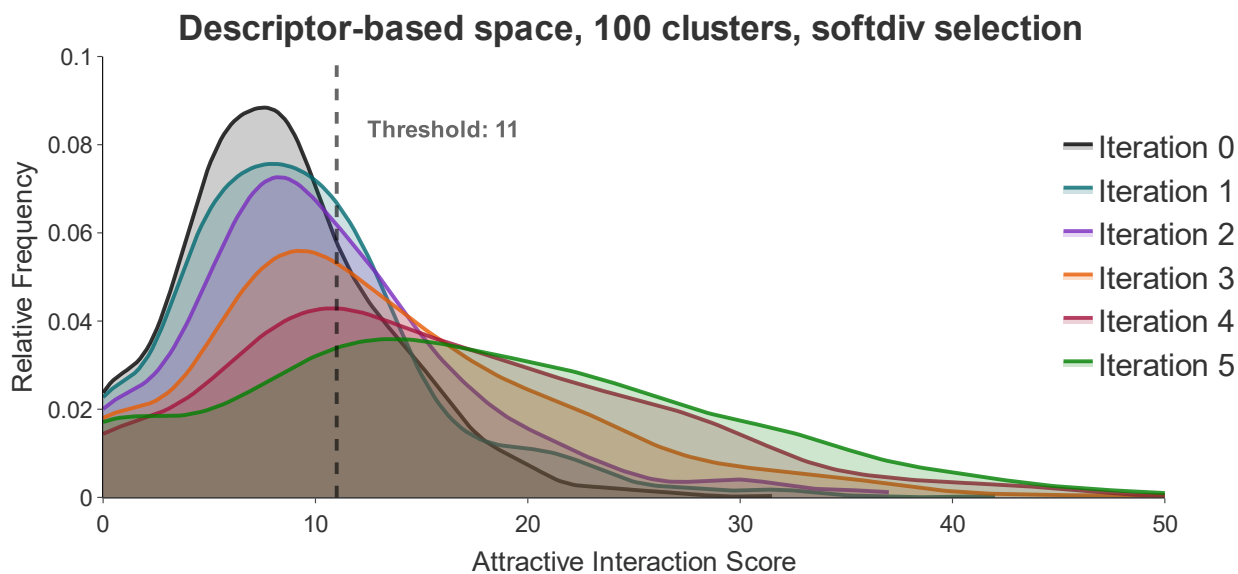


**Figure S4.2.** Attractive interaction scores for molecules generated by the pretrained model (iteration 0) and by the model after each of the five iterations of active learning where, prior to sampling for docking, molecules in the chemical space are grouped into 100 clusters, and cluster scores are converted into sampling fractions using the *softdiv* approach.

**Table S4-3.** Statistics of the distribution of attractive interaction scores, when molecules are selected randomly (naïve active learning), with no clustering.

Iteration	Percent > 11	Q1	Q2	Mean	Q3	Max	Std
0	26.20	5.50	8.00	8.41	11.00	33.00	4.58
1	32.40	5.50	9.00	9.27	11.50	35.00	4.79
2	35.00	6.50	9.00	9.67	12.50	33.00	4.89
3	40.00	6.88	9.50	10.45	13.50	37.00	5.31
4	44.80	7.00	10.00	11.03	13.63	42.00	6.16
5	44.20	7.00	10.00	11.13	13.50	38.50	6.05

<sup>a</sup> The percentage of generated molecules with attractive interaction scores equal to or above our score threshold is shown (Percent > 11), as well as the score at the first quartile (Q1), second quartile (Q2), Mean, third quartile (Q3), maximum (Max), and standard deviation (Std) of the distribution.

<sup>b</sup> Iteration 0 refers to the pretraining phase, while later iterations refer to the active learning phases.

<sup>c</sup> This table corresponds to the distribution in Figure 4A of main text.

**Table S4.4.** Statistics of the distribution of attractive interaction scores, when molecules are clustered into 100 groups and cluster scores are sampled *uniformly*.

Iteration	Percent > 11	Q1	Q2	Mean	Q3	Max	Std
0	12.00	6.68	8.58	8.43	9.85	15.80	2.31
1	24.00	7.75	9.10	9.17	10.88	20.80	3.40
2	30.00	8.17	9.40	9.96	11.50	21.50	3.41
3	35.00	7.86	10.07	10.23	11.63	24.00	3.97
4	50.00	8.88	10.89	11.28	13.46	25.45	4.11
5	50.00	8.80	10.94	11.84	14.48	25.80	4.63

<sup>a</sup> The percentage of generated molecules with attractive interaction scores equal to or above our score threshold is shown (Percent > 11), as well as the score at the first quartile (Q1), second quartile (Q2), Mean, third quartile (Q3), maximum (Max), and standard deviation (Std) of the distribution.

<sup>b</sup> Iteration 0 refers to the pretraining phase, while later iterations refer to the active learning phases.

<sup>c</sup> This table corresponds to the distribution in Figure 4B of main text.

**Table S4.5.** Statistics of the distribution of attractive interaction scores, when molecules are clustered into 100 groups and cluster scores are converted into sampling fractions using the *linear* method.

Iteration	Percent > 11	Q1	Q2	Mean	Q3	Max	Std
0	12.00	6.68	8.58	8.43	9.85	15.80	2.31
1	23.23	7.88	9.20	9.54	10.71	19.95	2.73
2	37.00	7.78	9.98	10.24	12.10	26.25	4.40
3	47.00	8.29	10.55	11.60	14.51	23.90	5.09
4	62.00	10.19	13.27	13.19	15.84	31.41	5.09
5	71.00	10.50	13.43	14.00	16.93	29.50	5.50

<sup>a</sup> The percentage of generated molecules with attractive interaction scores equal to or above our score threshold is shown (Percent > 11), as well as the score at the first quartile (Q1), second quartile (Q2), Mean, third quartile (Q3), maximum (Max), and standard deviation (Std) of the distribution.

<sup>b</sup> Iteration 0 refers to the pretraining phase, while later iterations refer to the active learning phases.

<sup>c</sup> This table corresponds to the distribution in Figure S4.1.

**Table S4.6.** Statistics of the distribution of attractive interaction scores, when molecules are clustered into 100 groups and cluster scores are converted into sampling fractions using the *softdiv* method.

Iteration	Percent > 11	Q1	Q2	Mean	Q3	Max	Std
0	28.10	5.50	8.00	8.46	11.50	31.50	4.89
1	34.70	5.50	8.50	9.29	12.50	42.00	5.89
2	42.20	6.50	9.50	10.54	13.50	37.00	6.64
3	54.20	7.50	11.50	13.07	18.00	55.00	8.64
4	65.90	8.50	14.25	15.82	22.00	56.50	9.99
5	71.20	9.50	16.00	17.32	24.50	51.00	10.90

<sup>a</sup> The percentage of generated molecules with attractive interaction scores equal to or above our score threshold is shown (Percent > 11), as well as the score at the first quartile (Q1), second quartile (Q2), Mean, third quartile (Q3), maximum (Max), and standard deviation (Std) of the distribution.

<sup>b</sup> Iteration 0 refers to the pretraining phase, while later iterations refer to the active learning phases.

<sup>c</sup> This table corresponds to the distribution in Figure S4.2.

## Section 5: Evolution of the distribution of the number of attractive interactions for different conversion methods

Interaction Counts per 1000 Molecules (Random Sampling)

	CationPi	EdgeToFace	FaceToFace	Hydrogen-bond	Hydrophobic	Ionic	MetalAcceptor	PiCation	Van der Waals	XBDonor
PDB Bind	44.0	131.0	209.0	3684.0	7434.0	763.0	101.0	37.0	9974.0	20.0
Iteration 0	0.0	18.0	3.0	162.0	1507.0	45.0	0.0	5.0	3701.0	17.0
Iteration 1	0.0	13.0	3.0	167.0	1751.0	60.0	0.0	4.0	3749.0	27.0
Iteration 2	0.0	24.0	5.0	142.0	1859.0	76.0	0.0	12.0	3813.0	24.0
Iteration 3	0.0	19.0	8.0	139.0	2002.0	121.0	0.0	5.0	3925.0	24.0
Iteration 4	0.0	23.0	3.0	168.0	2028.0	183.0	0.0	7.0	3881.0	22.0
Iteration 5	0.0	25.0	4.0	167.0	2053.0	172.0	0.0	8.0	3992.0	24.0

**Figure S5.1.** Counts of interactions of each type for 1000 scored molecules generated by the pretrained model (iteration 0) and by the model after each of the five rounds of naïve active learning with *random sampling*. A count of interactions from 1000 protein-ligand complexes randomly sampled from the refined set of PDBbind v2020 is included for comparison. These counts correspond to the score distribution in Figure 4A of main text.

Interaction Counts per 1000 Molecules (Diffusion-based Sampling)

	CationPi	EdgeToFace	FaceToFace	Hydrogen-bond	Hydrophobic	Ionic	MetalAcceptor	PiCation	Van der Waals	XBDonor
PDB Bind	44.0	131.0	209.0	3684.0	7434.0	763.0	101.0	37.0	9974.0	20.0
Iteration 0	0.0	18.0	3.0	162.0	1507.0	45.0	0.0	5.0	3701.0	17.0
Iteration 1	0.0	18.0	1.0	193.0	1529.0	114.0	0.0	11.0	3890.0	10.0
Iteration 2	0.0	20.0	2.0	221.0	1543.0	155.0	0.0	9.0	4156.0	12.0
Iteration 3	0.0	7.0	2.0	231.0	1471.0	200.0	0.0	7.0	4234.0	16.0
Iteration 4	1.0	19.0	5.0	251.0	1530.0	288.0	0.0	9.0	4485.0	8.0
Iteration 5	3.0	17.0	1.0	255.0	1460.0	372.0	0.0	11.0	4584.0	16.0

**Figure S5.2.** Counts of interactions of each type for 1000 molecules generated by the pretrained model (iteration 0) and by the model after each of the five rounds of active learning with clustering into 100 groups and *uniform* selection from each cluster. A count of interactions from 1000 protein-ligand complexes randomly sampled from the refined set of PDBbind v2020 is included for comparison. These counts correspond to the score distribution in Figure 4B of main text.



Interaction Counts per 1000 Molecules (Linear-based Sampling)

	CationPi	EdgeToFace	FaceToFace	Hydrogen-bond	Hydrophobic	Ionic	MetalAcceptor	PiCation	Van der Waals	XBDonor
PDB Bind	44.0	131.0	209.0	3684.0	7434.0	763.0	101.0	37.0	9974.0	20.0
Iteration 0	0.0	18.0	3.0	162.0	1507.0	45.0	0.0	5.0	3701.0	17.0
Iteration 1	0.0	12.0	4.0	168.0	1630.0	116.0	0.0	9.0	3939.0	11.0
Iteration 2	0.0	14.0	2.0	207.0	1582.0	180.0	0.0	8.0	4075.0	15.0
Iteration 3	3.0	19.0	5.0	219.0	1666.0	316.0	0.0	7.0	4264.0	20.0
Iteration 4	1.0	11.0	4.0	222.0	1713.0	506.0	0.0	5.0	4579.0	13.0
Iteration 5	3.0	17.0	4.0	226.0	1691.0	618.0	0.0	10.0	4624.0	5.0

**Figure S5.3.** Counts of interactions of each type for 1000 scored molecules generated by the pretrained model (iteration 0) and by the model after each of the five rounds of active learning with clustering into 100 groups and conversion of cluster scores into sampling fractions using the *linear* method. A count of interactions from 1000 protein-ligand complexes randomly sampled from the refined set of PDBbind v2020 is included for comparison. These counts correspond to the score distribution in Figure S4.1.

Interaction Counts per 1000 Molecules (Softdiv-based Sampling)

	CationPi	EdgeToFace	FaceToFace	Hydrogen-bond	Hydrophobic	Ionic	MetalAcceptor	PiCation	Van der Waals	XBDonor
PDB Bind	44.0	131.0	209.0	3684.0	7434.0	763.0	101.0	37.0	9974.0	20.0
Iteration 0	0.0	18.0	3.0	162.0	1507.0	45.0	0.0	5.0	3701.0	17.0
Iteration 1	0.0	24.0	5.0	146.0	1269.0	93.0	0.0	6.0	3233.0	14.0
Iteration 2	0.0	16.0	4.0	213.0	1632.0	195.0	0.0	7.0	4170.0	12.0
Iteration 3	0.0	20.0	2.0	193.0	1762.0	476.0	0.0	7.0	4328.0	16.0
Iteration 4	5.0	21.0	6.0	211.0	1847.0	765.0	0.0	16.0	4589.0	14.0
Iteration 5	4.0	32.0	4.0	262.0	1708.0	974.0	0.0	21.0	4701.0	8.0

**Figure S5.4.** Counts of interactions of each type for 1000 scored molecules generated by the pretrained model (iteration 0) and by the model after each of the five rounds of active learning with clustering into 100 groups and conversion of cluster scores into sampling fractions using the *softdiv* method. A count of interactions from 1000 protein-ligand complexes randomly sampled from the refined set of PDBbind v2020 is included for comparison. These counts correspond to the score distribution in Figure S4.2.

Interaction Counts per 1000 Molecules (Softsub-based Sampling)

PDB Bind	44.0	131.0	209.0	3684.0	7434.0	763.0	101.0	37.0	9974.0	20.0
Iteration 0	0.0	18.0	3.0	162.0	1507.0	45.0	0.0	5.0	3701.0	17.0
Iteration 1	0.0	17.0	2.0	185.0	1656.0	99.0	0.0	6.0	4134.0	18.0
Iteration 2	1.0	15.0	2.0	187.0	1830.0	347.0	0.0	8.0	4321.0	7.0
Iteration 3	1.0	23.0	2.0	176.0	1857.0	724.0	0.0	10.0	4352.0	15.0
Iteration 4	1.0	19.0	5.0	152.0	1954.0	1104.0	0.0	6.0	4452.0	15.0
Iteration 5	2.0	39.0	5.0	161.0	2026.0	1291.0	0.0	8.0	4653.0	12.0
	CationPI	EdgeToFace	FaceToFace	Hydrogen-bond	Hydrophobic	Ionic	MetalAcceptor	PIcation	Van der Waals	XBDonor

**Figure S5.5.** Counts of interactions of each type for 1000 molecules generated by the pretrained model (iteration 0) and by the model after each of the five rounds of active learning with clustering into 100 groups and conversion of cluster scores into sampling fractions using the *softsub* method. A count of interactions from 1000 protein-ligand complexes randomly sampled from the refined set of PDBbind v2020 is included for comparison. These counts correspond to the score distribution in Figure 4C of the main text.

**Section 6: Evolution of the distribution of cluster-average attractive interaction scores for different conversion methods**

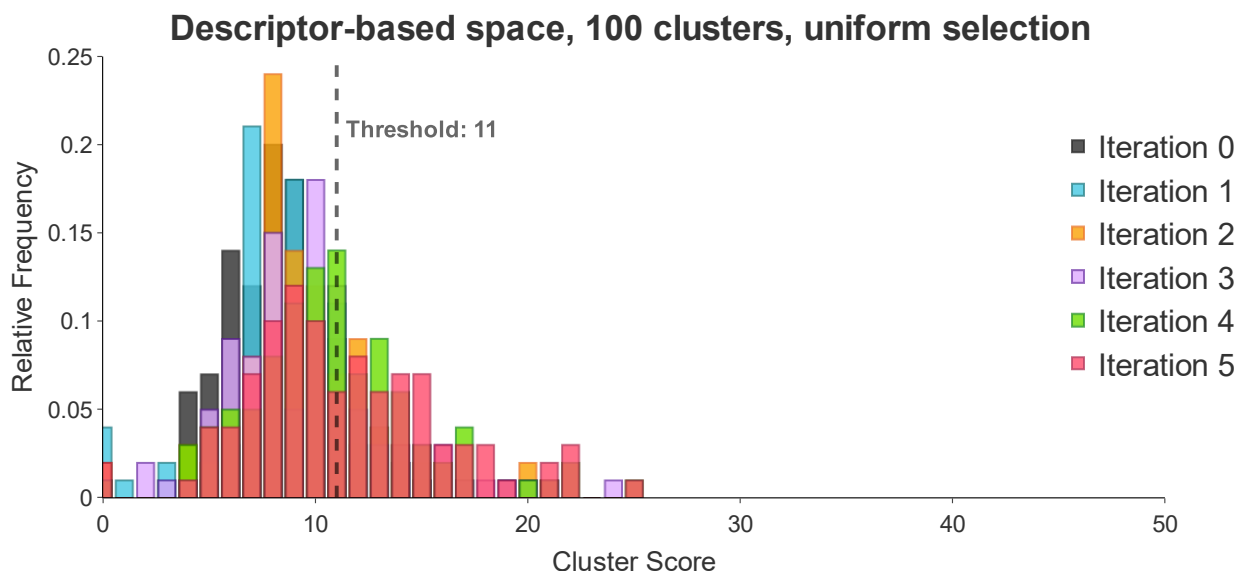


**Figure S6.1.** Cluster scores (obtained as an average of attractive interaction scores for molecules in the cluster) for molecules generated by the pretrained model (iteration 0) and by the model after each of the five iterations of active learning where, prior to sampling for docking, molecules in the chemical space are grouped into 100 clusters, and molecules are sampled from each cluster *uniformly*. These cluster scores correspond to score distribution in Figure 4B of the main text.

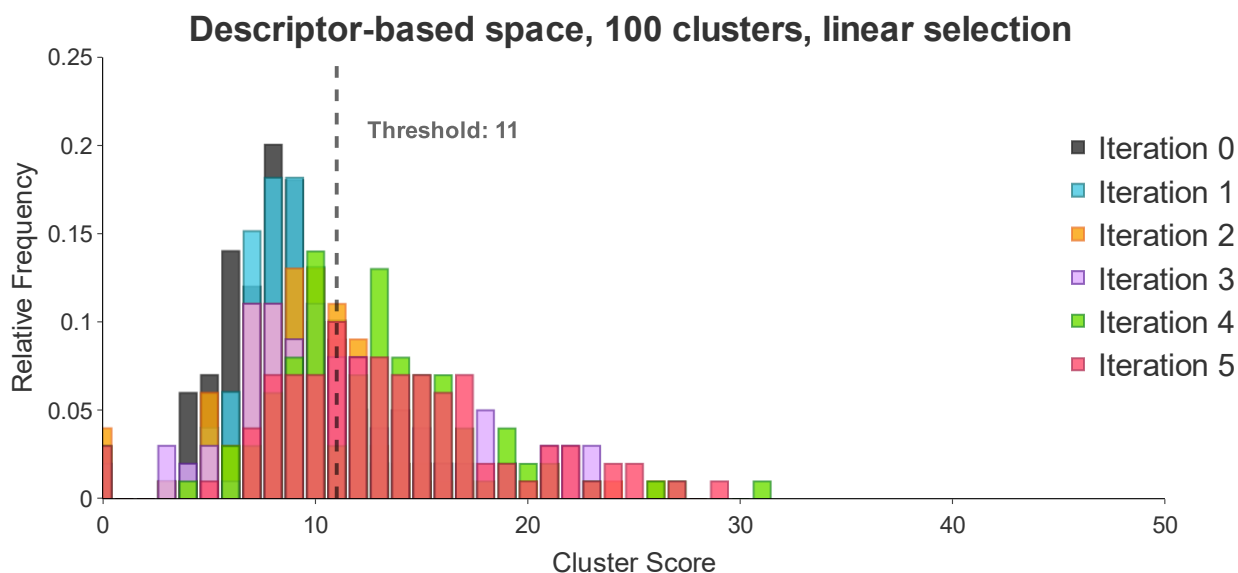


**Figure S6.2.** Cluster scores (obtained as an average of attractive interaction scores for molecules in the cluster) for molecules generated by the pretrained model (iteration 0) and by the model after each of the five iterations of active learning where, prior to sampling for docking, molecules in the chemical space are grouped into 100 clusters, and molecules are sampled from each cluster using the *linear* method. These cluster scores correspond to score distribution in Figure SI4.1.

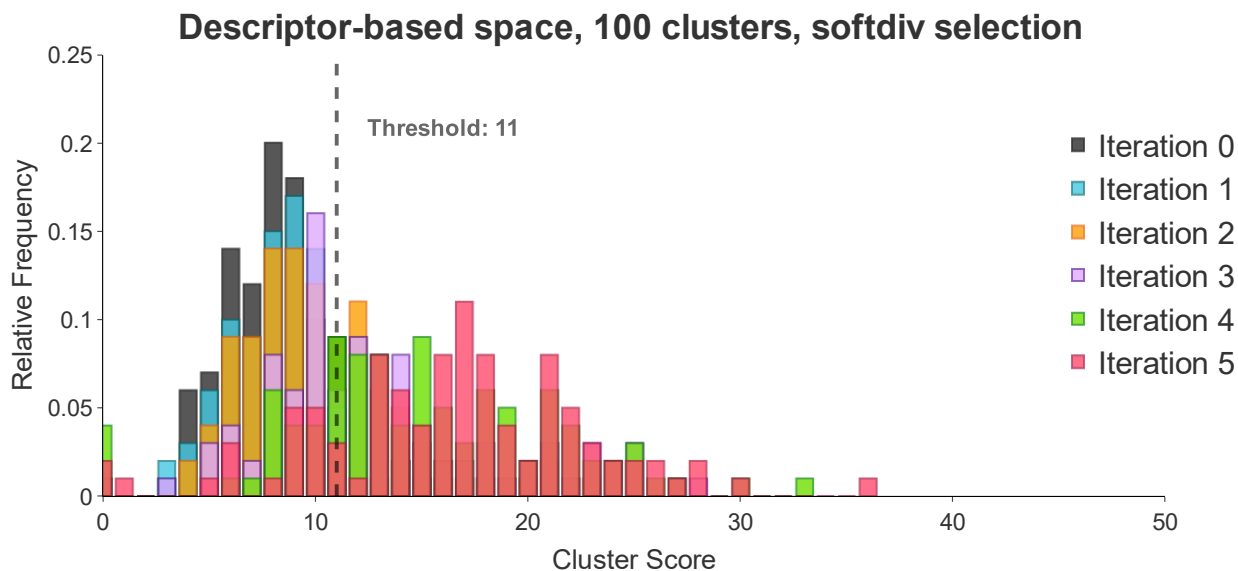


**Figure S6.3.** Cluster scores (obtained as an average of attractive interaction scores for molecules in the cluster) for molecules generated by the pretrained model (iteration 0) and by the model after each of the five iterations of active learning where, prior to sampling for docking, molecules in the chemical space are grouped into 100 clusters, and molecules are sampled from each cluster using the *softdiv* method. These cluster scores correspond to score distribution in Figure SI4.2.

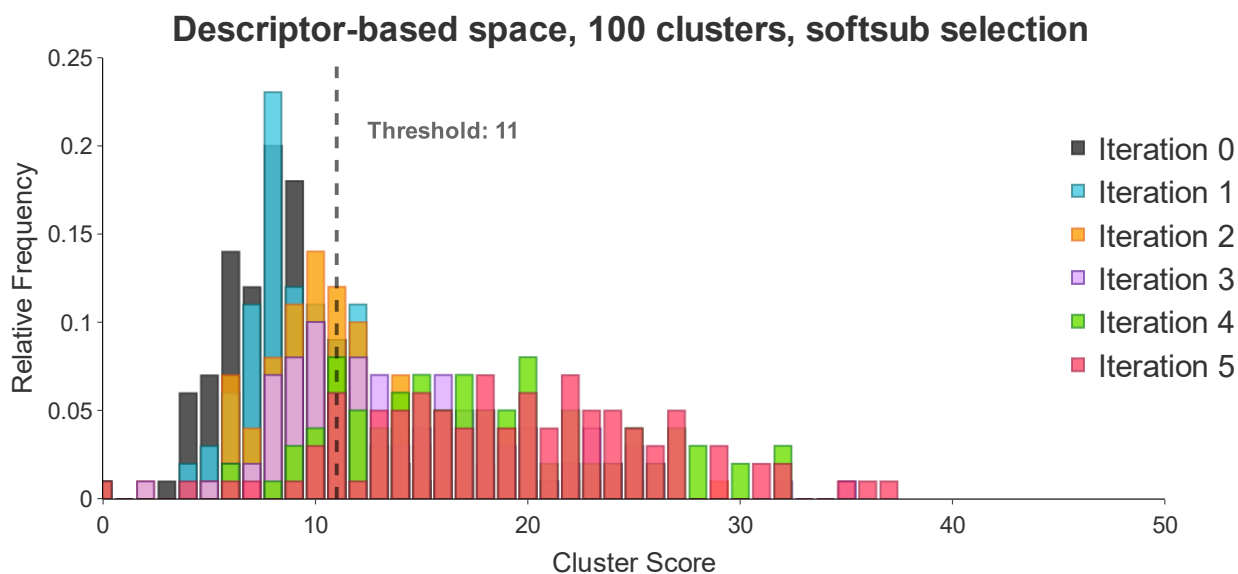


**Figure S6.4.** Cluster scores (obtained as an average of attractive interaction scores for molecules in the cluster) for molecules generated by the pretrained model (iteration 0) and by the model after each of the five iterations of active learning where, prior to sampling for docking, molecules in the chemical space are grouped into 100 clusters, and molecules are sampled from each cluster using the *softsub* method. These cluster scores correspond to score distribution in Figure 4C of the main text.

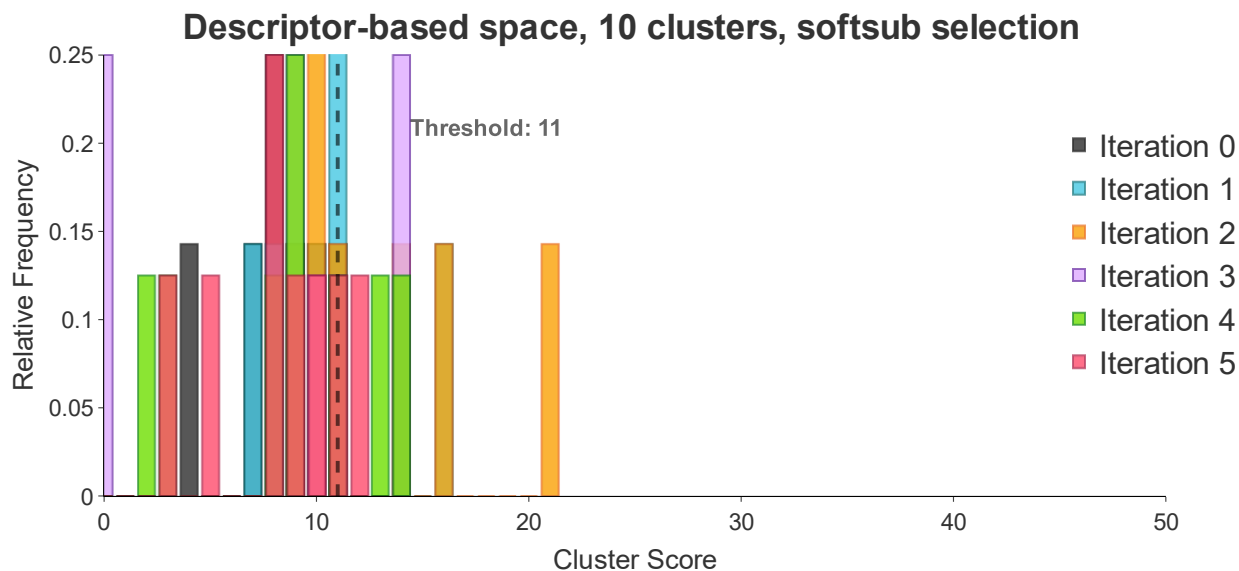


**Figure S6.5.** Cluster scores (obtained as an average of attractive interaction scores for molecules in the cluster) for molecules generated by the pretrained model (iteration 0) and by the model after each of the five iterations of active learning where, prior to sampling for docking, molecules in the chemical space are grouped into 10 clusters, and molecules are sampled from each cluster using the *softsub* method. These cluster scores correspond to score distribution in Figure S10.1 of the main text.

## Section 7: Performance on the MOSES benchmark

**Table S7.1.** Primary results of our pretrained model on the MOSES benchmark compared to top-performing models in the field.

Model	Validity	Unique@1K	Unique@10K	Novelty	IntDiv <sub>1</sub>	IntDiv <sub>2</sub>	Filters
<b><i>Our Model</i></b>	0.996	<b>1.000</b>	0.999	0.730	0.856	0.850	<b>0.998</b>
MolGPT <sup>69</sup>	0.994	N/A	<b>1.000</b>	0.797	0.857	0.851	N/A
LatentGAN <sup>70</sup>	0.897	<b>1.000</b>	0.997	0.949	0.857	0.850	0.973
JT-VAE <sup>50</sup>	<b>1.000</b>	<b>1.000</b>	<b>1.000</b>	0.914	0.855	0.849	0.976
CharRNN <sup>5</sup>	0.975	<b>1.000</b>	0.999	0.842	0.856	0.850	0.994
MolecularRNN <sup>26</sup>	<b>1.000</b>	N/A	0.994	<b>1.000</b>	0.881	<b>0.876</b>	N/A
iPPIgAN <sup>33</sup>	0.989	<b>1.000</b>	0.999	0.990	N/A	N/A	N/A
DNMG <sup>34</sup>	0.999	<b>1.000</b>	0.998	0.936	0.856	0.850	0.996
CogMol <sup>43</sup>	0.955	<b>1.000</b>	<b>1.000</b>	N/A	0.857	0.851	0.989
TransVAE <sup>51</sup>	0.567	NA	N/A	0.996	N/A	N/A	N/A
ShapeProb <sup>57</sup>	0.969	<b>1.000</b>	0.995	N/A	0.865	N/A	0.865
GENTRL <sup>54</sup>	0.850	N/A	N/A	N/A	N/A	N/A	N/A
TransAntivirus <sup>62</sup>	<b>1.000</b>	0.999	0.999	0.999	<b>0.895</b>	N/A	N/A
CRTmaccs <sup>64</sup>	<b>1.000</b>	<b>1.000</b>	<b>1.000</b>	<b>1.000</b>	N/A	N/A	N/A
MolGCT <sup>66</sup>	0.985	<b>1.000</b>	0.998	0.814	0.853	N/A	0.996
cMolGPT <sup>99</sup>	0.988	<b>1.000</b>	0.999	N/A	N/A	N/A	N/A
GraphINVENT <sup>77</sup>	0.964	<b>1.000</b>	0.998	N/A	0.857	0.851	0.950
cTransformer <sup>67</sup>	0.988	<b>1.000</b>	0.999	N/A	N/A	N/A	N/A
GMTransformer <sup>63</sup>	0.829	<b>1.000</b>	<b>1.000</b>	0.883	0.856	N/A	0.980

<sup>a</sup> Validity (ratio of generated molecules deemed valid by RDKit’s molecular structure parser), Unique@1K and @10K (fraction of valid generated molecules with no duplicates), Novelty (fraction of valid and unique generated molecules that are not in the training set), IntDiv<sub>*i*</sub> (internal diversity within the generated set for power mean *i*), and Filters (fraction of generated molecules that pass filters that check for specific fragments) are shown. See MOSES benchmark<sup>91</sup> for more details on how these metrics are calculated.

<sup>b</sup> The top value for each metric is shown in bold.

<sup>c</sup> Values not reported are shown as N/A.

**Table S7.2.** Additional results of our pretrained model on the MOSES benchmark compared to top-performing models in the field.

Model	FCD/Test	FCD/TestSF	Frag/Test	Frag/TestSF	SNN/Test	SNN/TestSF	Scaff/Test	Scaff/TestSF
<b>Our Model</b>	<b>0.038</b>	<b>0.450</b>	<b>1.000</b>	<b>0.999</b>	0.633	<b>0.585</b>	<b>0.970</b>	0.071
MolGPT <sup>69</sup>	0.067	0.507	N/A	N/A	N/A	N/A	N/A	N/A
LatentGAN <sup>70</sup>	0.296	0.824	0.999	0.998	0.538	0.514	0.886	0.100
JT-VAE <sup>50</sup>	0.395	0.938	0.997	0.995	0.548	0.519	0.896	0.101
CharRNN <sup>5</sup>	0.073	0.520	<b>1.000</b>	0.998	0.601	0.565	0.924	0.110
MolecularRNN <sup>26</sup>	N/A	N/A	N/A	N/A	N/A	N/A	N/A	N/A
iPPIgAN <sup>33</sup>	5.879	6.171	N/A	N/A	N/A	N/A	N/A	N/A
DNMG <sup>34</sup>	0.373	0.631	0.999	0.998	0.472	0.579	0.784	<b>0.998</b>
CogMol <sup>43</sup>	0.166	0.603	0.999	0.997	0.560	0.533	0.905	0.128
TransVAE <sup>51</sup>	N/A	N/A	N/A	N/A	N/A	N/A	N/A	N/A
ShapeProb <sup>57</sup>	1.332	1.850	0.984	0.980	0.446	0.432	0.459	0.066
GENTRL <sup>54</sup>	N/A	N/A	N/A	N/A	N/A	N/A	N/A	N/A
TransAntivirus <sup>62</sup>	10.947	N/A	N/A	N/A	N/A	N/A	N/A	N/A
CRTmaccs <sup>64</sup>	13.565	13.999	N/A	N/A	0.334	0.330	N/A	N/A
MolGCT <sup>66</sup>	0.402	0.803	0.997	0.995	0.618	0.577	0.891	0.092
cMolGPT <sup>99</sup>	N/A	N/A	<b>1.000</b>	0.998	0.619	0.578	N/A	N/A
GraphINVENT <sup>77</sup>	0.682	1.223	0.986	0.986	0.569	0.539	0.885	0.127
cTransformer <sup>67</sup>	N/A	N/A	<b>1.000</b>	0.998	0.619	0.578	N/A	N/A
GMTransformer <sup>63</sup>	0.199	0.760	0.998	0.996	0.578	0.546	0.913	0.109

<sup>a</sup> FCD (Fréchet ChemNet Distance that is calculated using activation of the penultimate layer of ChemNet), Frag (compares molecular fragments between generated and training sets), SNN (average Tanimoto similarity between molecules in the generated set and the corresponding nearest molecule in the training set), and Scaff (compares molecular scaffolds between generated and training sets) are shown. Test (similarity from the training set to the test set) and TestSF (similarity from the training set to the scaffold test set) are shown for each metric. See MOSES benchmark<sup>91</sup> for more details on how these metrics are calculated

<sup>b</sup> The top value for each metric is shown in bold.

<sup>c</sup> Values not reported are shown as N/A

## **Section 8: Details on the execution of t-distributed stochastic neighbor embedding (t-SNE)**

To create a standard t-SNE space which involves a constant coordinate system, we proceed as follows. Firstly, we collect scored molecules from all iterations (6,000 molecules). Secondly, we add the molecules from all active learning training sets that employed either softmax or uniform selection methods. Thirdly, we add a random sample of 10,000 molecules from the set of generations at each iteration. We perform this sampling to have the same number of molecules from the active learning training sets and generated sets, which enables us to fairly compute the difference in distributions. Note that our training sets usually contain slightly more than 10,000 molecules, so we sample exactly 10,000 for consistency. After combining all molecules and dropping all duplicates, we perform a t-SNE reduction.



**Section 9: Vocabulary composition of the combined dataset**

**Table S9.1.** List of unique tokens that occur in the unfiltered combined dataset less than 1,000 times.

- '%10'	- '[125IH]'	- '[32P]'	- '[Be+2]'
- '%11'	- '[125I]'	- '[35S]'	- '[Bi+3]'
- '%12'	- '[127I]'	- '[3H]'	- '[BiH3]'
- '%13'	- '[127Xe]'	- '[42K+]'	- '[Bi]'
- '%14'	- '[129Xe]'	- '[45Ca+2]'	- '[Br+2]'
- '%15'	- '[131Cs]'	- '[47Ca+2]'	- '[Br]'
- '%16'	- '[131I-]'	- '[4H]'	- '[C+]'
- '%17'	- '[131I]'	- '[73Se]'	- '[CH+]'
- '%18'	- '[133Xe]'	- '[75Se]'	- '[CH-]'
- '%19'	- '[135I]'	- '[76BrH]'	- '[CH2+]'
- '%20'	- '[13CH2]'	- '[76Br]'	- '[CH2-]'
- '%21'	- '[13CH3]'	- '[81Kr]'	- '[CH2]'
- '%22'	- '[13CH]'	- '[82Rb+]'	- '[CH]'
- '%23'	- '[13C]'	- '[82Rb]'	- '[C]'
- '%24'	- '[13NH3]'	- '[85Sr+2]'	- '[Ca++]'
- '%25'	- '[13cH]'	- '[85SrH2]'	- '[Ca+2]'
- '%26'	- '[13c]'	- '[89Sr+2]'	- '[CaH2]'
- '%27'	- '[14C@@H]'	- '[Ag+]'	- '[Ca]'
- '%28'	- '[14C@@]'	- '[Ag-4]'	- '[Cl+2]'
- '%29'	- '[14C@H]'	- '[Ag-]'	- '[Cl+3]'
- '%30'	- '[14CH2]'	- '[Ag]'	- '[Cl+]'
- '%31'	- '[14CH3]'	- '[Al+3]'	- '[Cl]'
- '%32'	- '[14CH]'	- '[Al-3]'	- '[Co]'
- '*'	- '[14C]'	- '[Al]'	- '[Cs+]'
- ':'	- '[14cH]'	- '[Ar]'	- '[Cs]'
- '[*]'	- '[14c]'	- '[As+]'	- '[Cu-]'
- '[10B]'	- '[15NH]'	- '[As-]'	- '[Cu]'
- '[11C-]'	- '[15OH2]'	- '[AsH3]'	- '[F+]'
- '[11C@@H]'	- '[15nH]'	- '[AsH]'	- '[F-]'
- '[11CH2]'	- '[15n]'	- '[As]'	- '[Fe++]'
- '[11CH3]'	- '[17F]'	- '[At]'	- '[Fe--]'
- '[11CH]'	- '[18F-]'	- '[Au-]'	- '[Fe-3]'
- '[11C]'	- '[18FH]'	- '[Au]'	- '[Fe]'
- '[11c]'	- '[18F]'	- '[B@-]'	- '[Gd-4]'
- '[123I-]'	- '[18OH]'	- '[B@@-]'	- '[Gd-5]'
- '[123IH]'	- '[18O]'	- '[BH-]'	- '[H+]'
- '[123I]'	- '[19F]'	- '[BH2-]'	- '[H-]'
- '[123Te]'	- '[211At]'	- '[BH3-]'	- '[HH]'
- '[124I-]'	- '[223Ra]'	- '[B]'	- '[He]'
- '[124I]'	- '[22Na+]'	- '[Ba+2]'	- '[Hg]'
- '[125I-]'	- '[32PH]'	- '[Ba]'	- '[I+2]'

- '[I+3]'	- '[Ni++]'	- '[S-]'	- '[TeH]'
- '[I+]	- '[Ni]'	- '[S@+]'	- '[Te]'
- '[IH2]'	- '[O+]'	- '[S@@+]'	- '[V]'
- '[IH]'	- '[O-2]'	- '[S@]'	- '[W]'
- '[I]'	- '[OH+]'	- '[SH+]'	- '[Xe]'
- '[KH]'	- '[OH-]'	- '[SH-]'	- '[Zn++]'
- '[K]'	- '[OH]'	- '[SH2]'	- '[Zn+2]'
- '[Kr]'	- '[O]'	- '[SH]'	- '[Zn+]'
- '[Li+]'	- '[Os]'	- '[S]'	- '[Zn-2]'
- '[LiH]'	- '[P-]'	- '[Sb]'	- '[Zn]'
- '[Li]'	- '[P@+]'	- '[Se+]'	- '[b-]'
- '[Mg+2]'	- '[P@@+]'	- '[Se-2]'	- '[c+]'
- '[Mg+]'	- '[P@@]'	- '[Se-]'	- '[c-]'
- '[MgH2]'	- '[P@]'	- '[SeH2]'	- '[cH+]'
- '[Mg]'	- '[PH+]'	- '[SeH]'	- '[cH-]'
- '[Mn]'	- '[PH2+]'	- '[Si-]'	- '[c]'
- '[Mo]'	- '[PH2]'	- '[Si@]'	- '[n-]'
- '[N@+]'	- '[PH]'	- '[SiH-]'	- '[nH+]'
- '[N@@+]'	- '[P]'	- '[SiH2]'	- '[n]'
- '[N@@H+]'	- '[Pd--]'	- '[SiH3-]'	- '[o+]'
- '[N@@]'	- '[Pd]'	- '[SiH3]'	- '[o]'
- '[N@H+]'	- '[Pt--]'	- '[SiH4]'	- '[s+]'
- '[N@]'	- '[Pt]'	- '[SiH]'	- '[s]'
- '[NH-]'	- '[Ra]'	- '[Sn]'	- '[se+]'
- '[NH2+]'	- '[Rb+]'	- '[Sr++]'	- '[te+]'
- '[NH4+]'	- '[Rb]'	- '[Sr+2]'	- '[te]'
- '[NH]'	- '[Re-]'	- '[SrH2]'	- 'b'
- '[N]'	- '[Re]'	- '[Tc]'	- 'p'
- '[NaH]'	- '[Ru-]'	- '[Te+]'	
- '[Na]'	- '[Ru]'	- '[Te-]'	
- '[Nb--]'	- '[S-2]'	- '[TeH2]'	

**Table S9.2.** List of unique tokens in the filtered combined dataset.

- '!	- '[Na+]
- '#'	- '[O-]
- '('	- '[P+]
- ')'	- '[S+]
- ':'	- '[S@@]
- '::'	- '[Se]
- '/'	- '[Si]
- '1'	- '[n+]
- '2'	- '[nH]
- '3'	- '[se]
- '4'	- '\'
- '5'	- 'c'
- '6'	- 'n'
- '7'	- 'o'
- '8'	- 's'
- '9'	- '~'
- '<'	
- '='	
- 'B'	
- 'Br'	
- 'C'	
- 'Cl'	
- 'F'	
- 'I'	
- 'N'	
- 'O'	
- 'P'	
- 'S'	
- '[2H]	
- '[B-]	
- '[Br-]	
- '[C-]	
- '[C@@H]	
- '[C@@]	
- '[C@H]	
- '[C@]	
- '[Cl-]	
- '[H]	
- '[I-]	
- '[K+]	
- '[N+]	
- '[N-]	
- '[NH+]	
- '[NH3+]	

## Section 10: Choosing the number of clusters to use for k-means

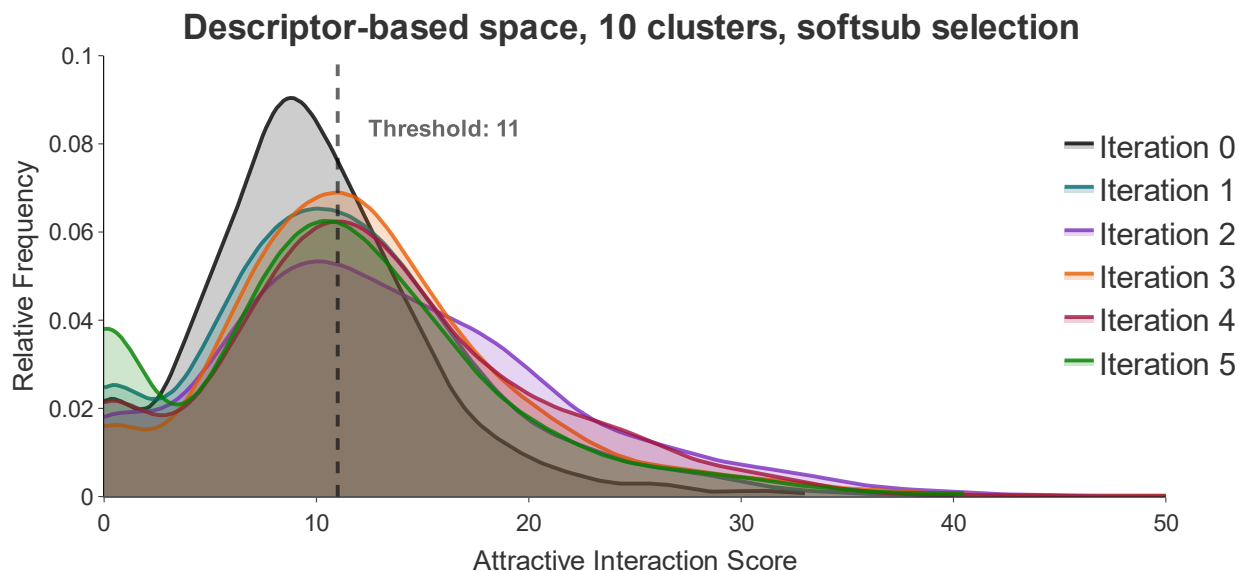


**Figure S10.1.** Attractive interaction scores for molecules generated by the pretrained model (iteration 0) and by the model after each of the five iterations of active learning where, prior to sampling for docking, molecules in the chemical space are grouped into 10 clusters. Cluster scores are converted into sampling fractions using the *softsub* approach.

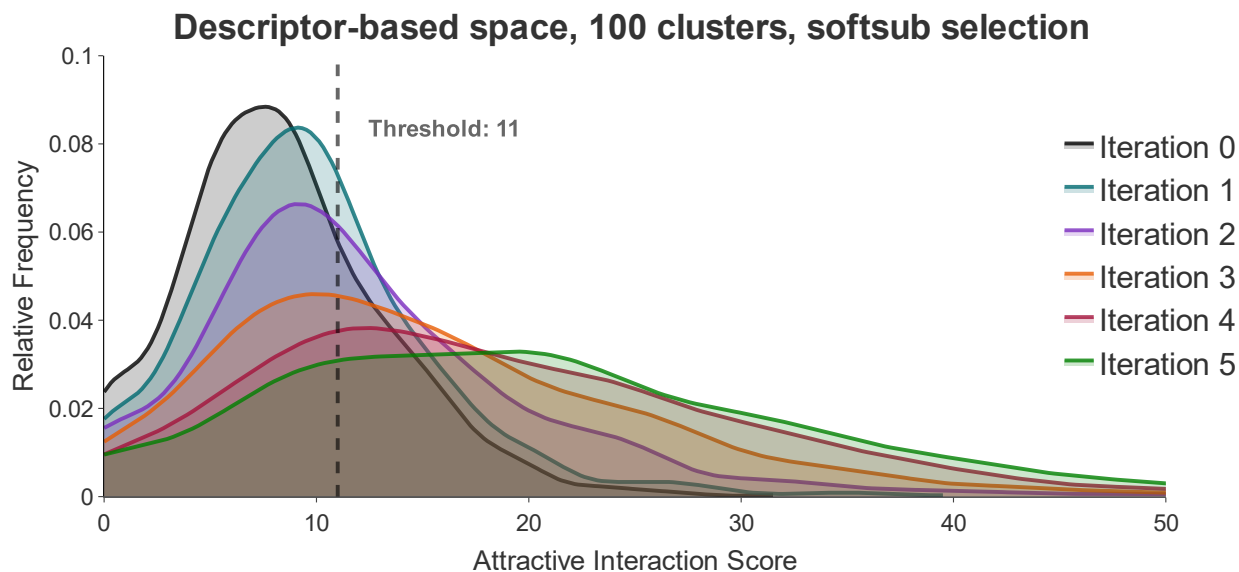


**Figure S10.2.** Attractive interaction scores for molecules generated by the pretrained model (iteration 0) and by the model after each of the five iterations of active learning where, prior to sampling for docking, molecules in the chemical space are grouped into 100 clusters. Cluster scores are converted into sampling fractions using the *softsub* approach. This figure occurs in the main text (Figure 4C), but is also shown here for comparison.

**Table S10.3.** Statistics of the distribution of attractive interaction scores, when molecules are clustered into 10 groups and cluster scores are converted into sampling fractions using the *softsub* method.

Iteration	Percent > 11	Q1	Q2	Mean	Q3	Max	Std
0	14.29	8.26	8.91	8.75	10.28	11.25	2.25
1	42.86	8.96	10.27	10.67	11.49	16.09	2.62
2	57.14	10.32	11.51	13.31	15.34	21.00	3.91
3	37.50	6.80	10.45	8.88	12.51	14.94	5.44
4	37.50	7.33	9.10	9.03	11.74	14.12	3.83
5	25.00	7.50	8.75	8.67	10.99	12.90	2.96

<sup>a</sup> The percentage of generated molecules with attractive interaction scores equal to or above our score threshold is shown (Percent > 11), as well as the score at the first quartile (Q1), second quartile (Q2), Mean, third quartile (Q3), maximum (Max), and standard deviation (Std) of the distribution.

<sup>b</sup> Iteration 0 refers to the pretraining phase, while later iterations refer to the active learning phases.

**Table S10.4.** Statistics of the distribution of attractive interaction scores, when molecules are clustered into 100 groups and cluster scores are converted into sampling fractions using the *softsub* method.

Iteration	Percent > 11	Q1	Q2	Mean	Q3	Max	Std
0	28.10	5.50	8.00	8.46	11.50	31.50	4.89
1	37.00	6.00	9.00	9.76	12.50	39.50	5.63
2	49.70	7.50	10.50	12.22	16.00	51.00	7.93
3	62.60	8.00	13.50	15.14	20.63	54.00	9.70
4	72.90	10.00	16.50	18.25	25.00	55.50	10.90
5	76.00	11.00	19.00	20.08	27.63	59.00	11.90

<sup>a</sup> The percentage of generated molecules with attractive interaction scores equal to or above our score threshold is shown (Percent > 11), as well as the score at the first quartile (Q1), second quartile (Q2), Mean, third quartile (Q3), maximum (Max), and standard deviation (Std) of the distribution.

<sup>b</sup> Iteration 0 refers to the pretraining phase, while later iterations refer to the active learning phases.

## Section 11: Additional evaluation of generations across active learning iterations

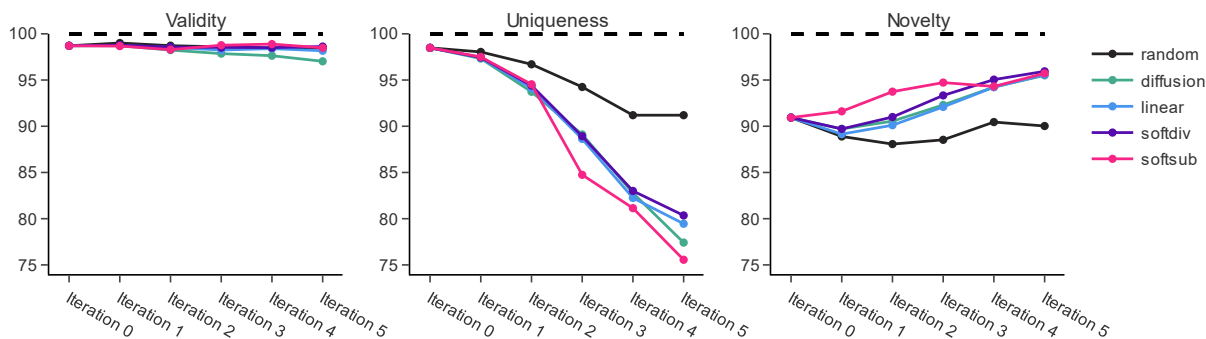


**Figure S11.1.** Percentage of molecules generated by our model that are valid, unique, or novel after pretraining (iteration 0) and five rounds of active learning. Data are shown for different sampling/conversion schemes.

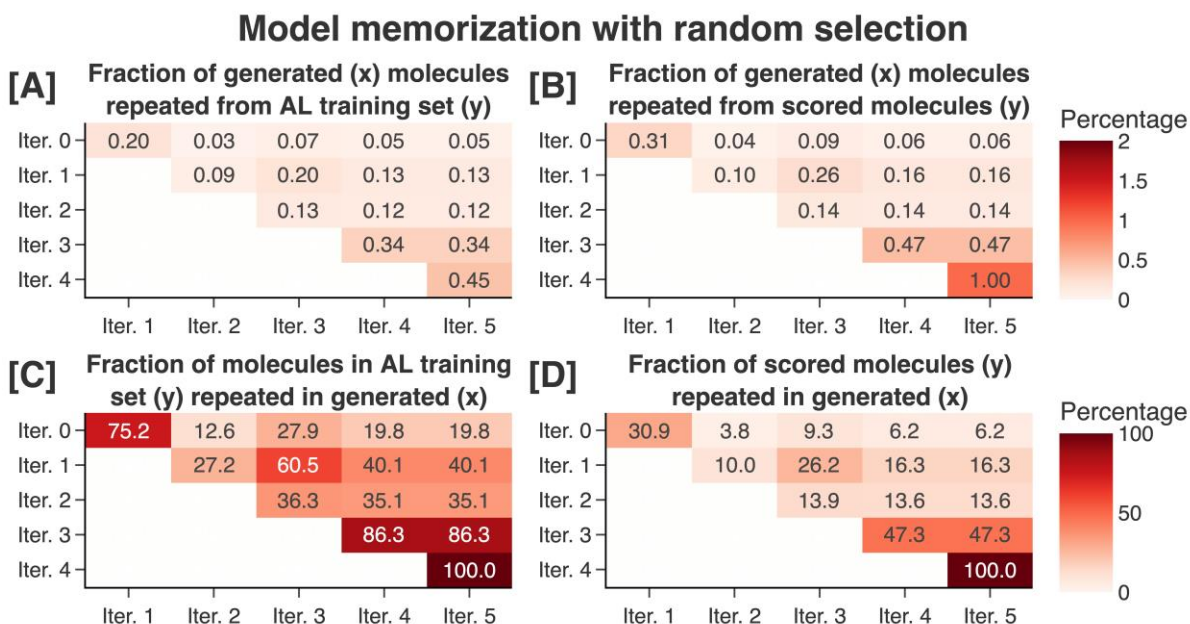


**Figure S11.2.** Memorization of training set by our model over five rounds of naïve active learning with random selection. (A) The fraction of molecules in a set of 100,000 generated at iteration  $i$  that occur in the training set at iteration  $i-1$ . (B) The fraction of molecules in a set of 100,000 generated at iteration  $i$  that occur in the set of scored molecules at iteration  $i-1$ . (C) The number of molecules from the active training set at iteration  $i-1$  that occurs in generations at iteration  $i$  divided by the size of the active learning training set at iteration  $i-1$ . (D) the number of scored molecules at iteration  $i-1$  that occur in generations at iteration  $i$  divided by number of scored molecules at iteration  $i-1$  (i.e., 1000).

## Model memorization with uniform selection

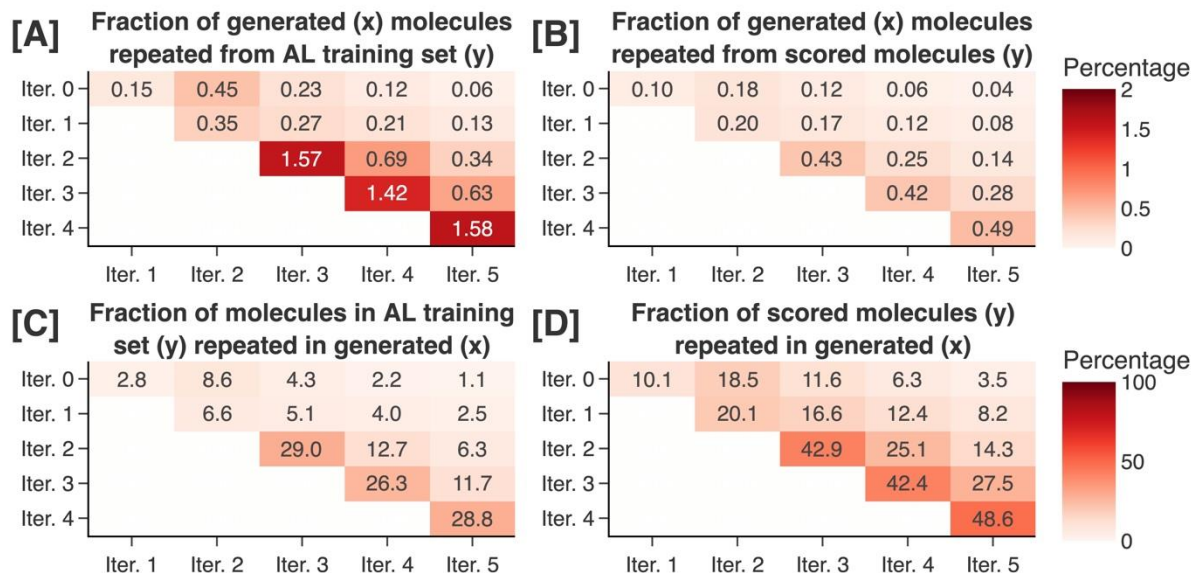


**Figure S11.3.** Memorization of training set by our model over five rounds of active learning with 100 clusters and uniform selection. (A) The fraction of molecules in a set of 100,000 generated at iteration  $i$  that occur in the training set at iteration  $i-1$ . (B) The fraction of molecules in a set of 100,000 generated at iteration  $i$  that occur in the set of scored molecules at iteration  $i-1$ . (C) The number of molecules from the active training set at iteration  $i-1$  that occurs in generations at iteration  $i$  divided by the size of the active learning training set at iteration  $i-1$ . (D) the number of scored molecules at iteration  $i-1$  that occur in generations at iteration  $i$  divided by number of scored molecules at iteration  $i-1$  (i.e., 1000).

## Model memorization with linear-based selection

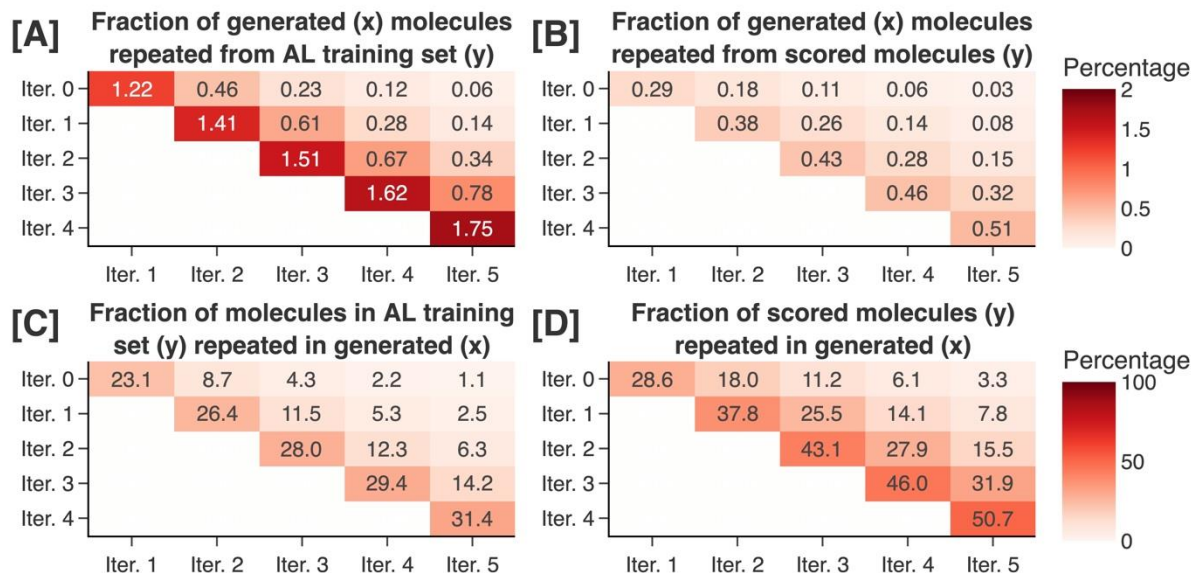


**Figure S11.4.** Memorization of training set by our model over five rounds of active learning with 100 clusters and linear selection. (A) The fraction of molecules in a set of 100,000 generated at iteration  $i$  that occur in the training set at iteration  $i-1$ . (B) The fraction of molecules in a set of 100,000 generated at iteration  $i$  that occur in the set of scored molecules at iteration  $i-1$ . (C) The number of molecules from the active training set at iteration  $i-1$  that occurs in generations at iteration  $i$  divided by the size of the active learning training set at iteration  $i-1$ . (D) the number of scored molecules at iteration  $i-1$  that occur in generations at iteration  $i$  divided by number of scored molecules at iteration  $i-1$  (i.e., 1000).



## Model memorization with softdiv-based selection

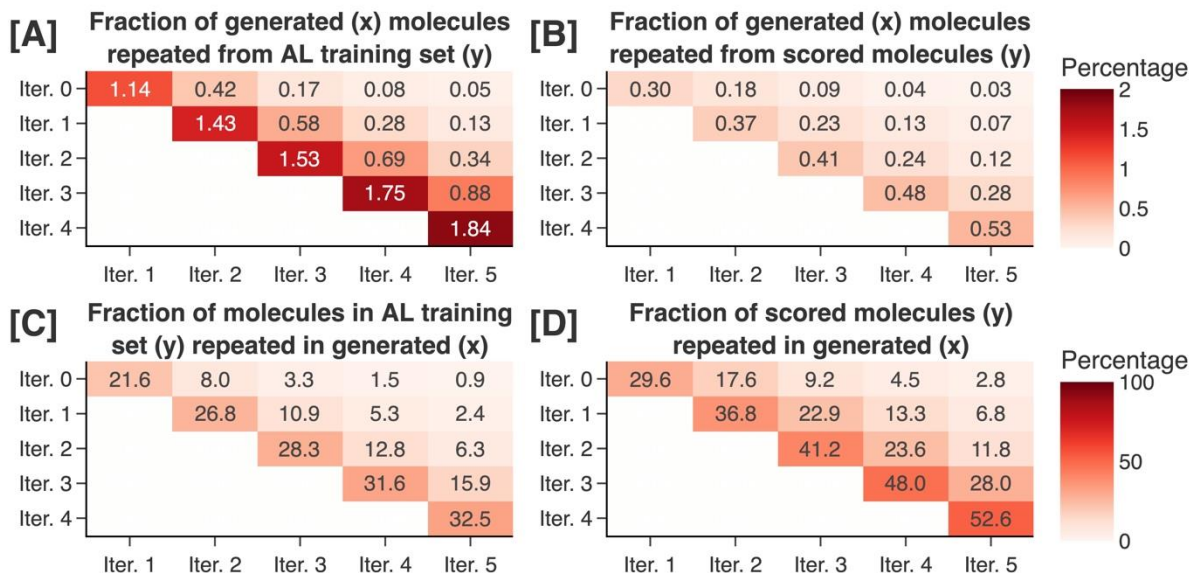


**Figure S11.5.** Memorization of training set by our model over five rounds of active learning with 100 clusters and softdiv selection. (A) The fraction of molecules in a set of 100,000 generated at iteration  $i$  that occur in the training set at iteration  $i-1$ . (B) The fraction of molecules in a set of 100,000 generated at iteration  $i$  that occur in the set of scored molecules at iteration  $i-1$ . (C) The number of molecules from the active training set at iteration  $i-1$  that occurs in generations at iteration  $i$  divided by the size of the active learning training set at iteration  $i-1$ . (D) the number of scored molecules at iteration  $i-1$  that occur in generations at iteration  $i$  divided by number of scored molecules at iteration  $i-1$  (i.e., 1000).

## Model memorization with softsub-based selection

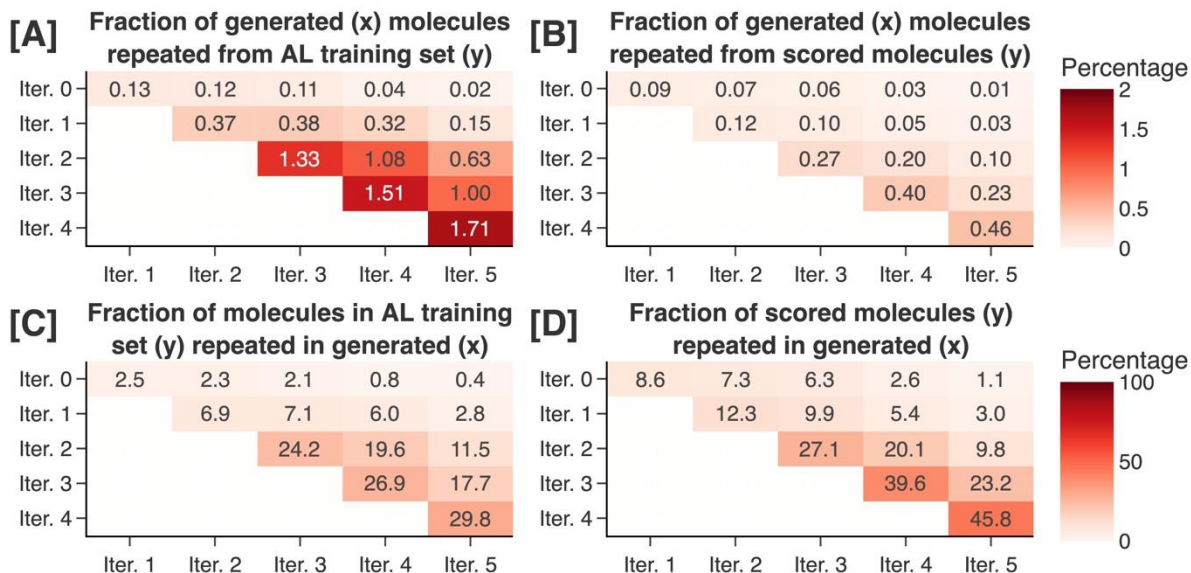


**Figure S11.6.** Memorization of training set by our model over five rounds of active learning with 100 clusters and softsub selection. (A) The fraction of molecules in a set of 100,000 generated at iteration  $i$  that occur in the training set at iteration  $i-1$ . (B) The fraction of molecules in a set of 100,000 generated at iteration  $i$  that occur in the set of scored molecules at iteration  $i-1$ . (C) The number of molecules from the active training set at iteration  $i-1$  that occurs in generations at iteration  $i$  divided by the size of the active learning training set at iteration  $i-1$ . (D) the number of scored molecules at iteration  $i-1$  that occur in generations at iteration  $i$  divided by number of scored molecules at iteration  $i-1$  (i.e., 1000).

## References

- <sup>1</sup> Shan, Y.; Kim, E. T.; Eastwood, M. P.; Dror, R. O.; Seeliger, M. A.; Shaw, D. E. How Does a Drug Molecule Find Its Target Binding Site? *Journal of the American Chemical Society* **2011**, *133* (24), 9181-9183. DOI: 10.1021/ja202726y.
- <sup>2</sup> Bilodeau, C.; Jin, W.; Jaakkola, T.; Barzilay, R.; Jensen, K. F. Generative models for molecular discovery: Recent advances and challenges. *WIREs Computational Molecular Science* **2022**, *12* (5), e1608, <https://doi.org/10.1002/wcms.1608>. DOI: <https://doi.org/10.1002/wcms.1608> (accessed 2023/05/09).
- <sup>3</sup> OpenAI. GPT-4 Technical Report. *ArXiv* **2023**, *abs/2303.08774*.
- <sup>4</sup> Jumper, J.; Evans, R.; Pritzel, A.; Green, T.; Figurnov, M.; Ronneberger, O.; Tunyasuvunakool, K.; Bates, R.; Žídek, A.; Potapenko, A.; et al. Highly accurate protein structure prediction with AlphaFold. *Nature* **2021**, *596* (7873), 583-589. DOI: 10.1038/s41586-021-03819-2.
- <sup>5</sup> Segler, M. H. S.; Kogej, T.; Tyrchan, C.; Waller, M. P. Generating Focused Molecule Libraries for Drug Discovery with Recurrent Neural Networks. *ACS Central Science* **2018**, *4* (1), 120-131. DOI: 10.1021/acscentsci.7b00512.
- <sup>6</sup> Urbina, F.; Lowden, C. T.; Culberson, J. C.; Ekins, S. MegaSyn: Integrating Generative Molecular Design, Automated Analog Designer, and Synthetic Viability Prediction. *ACS Omega* **2022**, *7* (22), 18699-18713. DOI: 10.1021/acsomega.2c01404.
- <sup>7</sup> Gupta, A.; Müller, A. T.; Huisman, B. J. H.; Fuchs, J. A.; Schneider, P.; Schneider, G. Generative Recurrent Networks for De Novo Drug Design. *Molecular Informatics* **2018**, *37* (1-2). DOI: 10.1002/minf.201700111.
- <sup>8</sup> Xu, M.; Ran, T.; Chen, H. De Novo Molecule Design Through the Molecular Generative Model Conditioned by 3D Information of Protein Binding Sites. *Journal of Chemical Information and Modeling* **2021**, *61* (7), 3240-3254. DOI: 10.1021/acs.jcim.0c01494.
- <sup>9</sup> Arús-Pous, J.; Blaschke, T.; Ulander, S.; Reymond, J.-L.; Chen, H.; Engkvist, O. Exploring the GDB-13 chemical space using deep generative models. *Journal of Cheminformatics* **2019**, *11* (1), 20. DOI: 10.1186/s13321-019-0341-z.
- <sup>10</sup> Yonchev, D.; Bajorath, J. DeepCOMO: from structure-activity relationship diagnostics to generative molecular design using the compound optimization monitor methodology. *Journal of Computer-Aided Molecular Design* **2020**, *34* (12), 1207-1218. DOI: 10.1007/s10822-020-00349-3.
- <sup>11</sup> Grisoni, F.; Moret, M.; Lingwood, R.; Schneider, G. Bidirectional Molecule Generation with Recurrent Neural Networks. *Journal of Chemical Information and Modeling* **2020**, *60* (3), 1175-1183. DOI: 10.1021/acs.jcim.9b00943.

- <sup>12</sup> Zhang, J.; Chen, H. De Novo Molecule Design Using Molecular Generative Models Constrained by Ligand–Protein Interactions. *Journal of Chemical Information and Modeling* **2022**, *62* (14), 3291-3306. DOI: 10.1021/acs.jcim.2c00177.
- <sup>13</sup> Arús-Pous, J.; Johansson, S. V.; Prykhodko, O.; Bjerrum, E. J.; Tyrchan, C.; Reymond, J.-L.; Chen, H.; Engkvist, O. Randomized SMILES strings improve the quality of molecular generative models. *Journal of Cheminformatics* **2019**, *11* (1), 71. DOI: 10.1186/s13321-019-0393-0.
- <sup>14</sup> Moret, M.; Friedrich, L.; Grisoni, F.; Merk, D.; Schneider, G. Generative molecular design in low data regimes. *Nature Machine Intelligence* **2020**, *2* (3), 171-180. DOI: 10.1038/s42256-020-0160-y.
- <sup>15</sup> Li, X.; Xu, Y.; Yao, H.; Lin, K. Chemical space exploration based on recurrent neural networks: applications in discovering kinase inhibitors. *Journal of Cheminformatics* **2020**, *12* (1), 42. DOI: 10.1186/s13321-020-00446-3.
- <sup>16</sup> Merk, D.; Friedrich, L.; Grisoni, F.; Schneider, G. De Novo Design of Bioactive Small Molecules by Artificial Intelligence. *Molecular Informatics* **2018**, *37* (1-2). DOI: 10.1002/minf.201700153.
- <sup>17</sup> Tan, X.; Jiang, X.; He, Y.; Zhong, F.; Li, X.; Xiong, Z.; Li, Z.; Liu, X.; Cui, C.; Zhao, Q.; et al. Automated design and optimization of multitarget schizophrenia drug candidates by deep learning. *European Journal of Medicinal Chemistry* **2020**, *204*, 112572. DOI: <https://doi.org/10.1016/j.ejmech.2020.112572>.
- <sup>18</sup> Bjerrum, E. J.; Threlfall, R. Molecular Generation with Recurrent Neural Networks (RNNs). *ArXiv* **2017**, *abs/1705.04612*.
- <sup>19</sup> Kotsias, P.-C.; Arús-Pous, J.; Chen, H.; Engkvist, O.; Tyrchan, C.; Bjerrum, E. J. Direct steering of de novo molecular generation with descriptor conditional recurrent neural networks. *Nature Machine Intelligence* **2020**, *2* (5), 254-265. DOI: 10.1038/s42256-020-0174-5.
- <sup>20</sup> Olivecrona, M.; Blaschke, T.; Engkvist, O.; Chen, H. Molecular de-novo design through deep reinforcement learning. *Journal of Cheminformatics* **2017**, *9* (1), 48. DOI: 10.1186/s13321-017-0235-x.
- <sup>21</sup> Popova, M.; Isayev, O.; Tropsha, A. Deep reinforcement learning for de novo drug design. *Science Advances* **2018**, *4* (7), eaap7885. DOI: [doi:10.1126/sciadv.aap7885](https://doi.org/10.1126/sciadv.aap7885).
- <sup>22</sup> Blaschke, T.; Engkvist, O.; Bajorath, J.; Chen, H. Memory-assisted reinforcement learning for diverse molecular de novo design. *Journal of Cheminformatics* **2020**, *12* (1), 68. DOI: 10.1186/s13321-020-00473-0.
- <sup>23</sup> Yoshimori, A.; Kawasaki, E.; Kanai, C.; Tasaka, T. Strategies for Design of Molecular Structures with a Desired Pharmacophore Using Deep Reinforcement Learning. *Chemical and Pharmaceutical Bulletin* **2020**, *68* (3), 227-233. DOI: 10.1248/cpb.c19-00625.

- <sup>24</sup> Blaschke, T.; Arús-Pous, J.; Chen, H.; Margreitter, C.; Tyrchan, C.; Engkvist, O.; Papadopoulos, K.; Patronov, A. REINVENT 2.0: An AI Tool for De Novo Drug Design. *Journal of Chemical Information and Modeling* **2020**, *60* (12), 5918-5922. DOI: 10.1021/acs.jcim.0c00915.
- <sup>25</sup> Korshunova, M.; Huang, N.; Capuzzi, S.; Radchenko, D. S.; Savych, O.; Moroz, Y. S.; Wells, C. I.; Willson, T. M.; Tropsha, A.; Isayev, O. Generative and reinforcement learning approaches for the automated de novo design of bioactive compounds. *Communications Chemistry* **2022**, *5* (1), 129. DOI: 10.1038/s42004-022-00733-0.
- <sup>26</sup> Popova, M.; Shvets, M.; Oliva, J.; Isayev, O. MolecularRNN: Generating realistic molecular graphs with optimized properties. *ArXiv* **2019**, *abs/1905.13372*.
- <sup>27</sup> Ghaemi, M. S.; Grantham, K.; Tamblyn, I.; Li, Y.; & Ooi, H. K. Generative Enriched Sequential Learning (ESL) Approach for Molecular Design via Augmented Domain Knowledge. *Proceedings of the Canadian Conference on Artificial Intelligence*, **2022**. DOI: <https://doi.org/10.21428/594757db.2a028ce5>
- <sup>28</sup> Wang, L.; Bai, R.; Shi, X.; Zhang, W.; Cui, Y.; Wang, X.; Wang, C.; Chang, H.; Zhang, Y.; Zhou, J.; et al. A pocket-based 3D molecule generative model fueled by experimental electron density. *Scientific Reports* **2022**, *12* (1), 15100. DOI: 10.1038/s41598-022-19363-6.
- <sup>29</sup> Bian, Y.; Wang, J.; Jun, J. J.; Xie, X. Q. Deep Convolutional Generative Adversarial Network (dcGAN) Models for Screening and Design of Small Molecules Targeting Cannabinoid Receptors. *Molecular Pharmaceutics* **2019**, *16* (11), 4451-4460. DOI: 10.1021/acs.molpharmaceut.9b00500.
- <sup>30</sup> Méndez-Lucio, O.; Baillif, B.; Clevert, D. A.; Rouquié, D.; Wichard, J. De novo generation of hit-like molecules from gene expression signatures using artificial intelligence. *Nature Communications* **2020**, *11* (1), 10. DOI: 10.1038/s41467-019-13807-w.
- <sup>31</sup> Cao, N. D.; Kipf, T. MolGAN: An implicit generative model for small molecular graphs. 2018. *ArXiv* **2018**, *abs/1805.11973*.
- <sup>32</sup> Tsujimoto, Y.; Hiwa, S.; Nakamura, Y.; Oe, Y.; Hiroyasu, T. L-MolGAN: An Improved Implicit Generative Model for Large Molecular Graphs. *ChemRxiv* **2021**. DOI: 10.26434/chemrxiv.14569545.v3.
- <sup>33</sup> Wang, J.; Chu, Y.; Mao, J.; Jeon, H.-N.; Jin, H.; Zeb, A.; Jang, Y.; Cho, K.-H.; Song, T.; No, K. T. De novo molecular design with deep molecular generative models for PPI inhibitors. *Briefings in Bioinformatics* **2022**, *23* (4), bbac285. DOI: 10.1093/bib/bbac285 (accessed 8/9/2023).
- <sup>34</sup> Song, T.; Ren, Y.; Wang, S.; Han, P.; Wang, L.; Li, X.; Rodriguez-Patón, A. DNMG: Deep molecular generative model by fusion of 3D information for de novo drug design. *Methods* **2023**, *211*, 10-22. DOI: <https://doi.org/10.1016/j.ymeth.2023.02.001>.

- <sup>35</sup> Bai, Q.; Tan, S.; Xu, T.; Liu, H.; Huang, J.; Yao, X. MolAICal: a soft tool for 3D drug design of protein targets by artificial intelligence and classical algorithm. *Briefings in Bioinformatics* **2021**, *22* (3). DOI: 10.1093/bib/bbaa161.
- <sup>36</sup> Putin, E.; Asadulaev, A.; Ivanenkov, Y.; Aladinskiy, V.; Sanchez-Lengeling, B.; Aspuru-Guzik, A.; Zhavoronkov, A. Reinforced Adversarial Neural Computer for de Novo Molecular Design. *Journal of Chemical Information and Modeling* **2018**, *58* (6), 1194-1204. DOI: 10.1021/acs.jcim.7b00690.
- <sup>37</sup> Lee, Y. J.; Kahng, H.; Kim, S. B. Generative Adversarial Networks for De Novo Molecular Design. *Molecular Informatics* **2021**, *40* (10), 2100045. DOI: <https://doi.org/10.1002/minf.202100045> (accessed 2023/08/09).
- <sup>38</sup> Sanchez-Lengeling, B.; Outeiral, C.; Guimaraes, G.; Aspuru-Guzik, A. Optimizing distributions over molecular space. An Objective-Reinforced Generative Adversarial Network for Inverse-design Chemistry (ORGANIC). *ChemRxiv* **2017**, DOI: 10.26434/chemrxiv.5309668.v3.
- <sup>39</sup> Putin, E.; Asadulaev, A.; Vanhaelen, Q.; Ivanenkov, Y.; Aladinskaya, A. V.; Aliper, A.; Zhavoronkov, A. Adversarial Threshold Neural Computer for Molecular de Novo Design. *Molecular Pharmaceutics* **2018**, *15* (10), 4386-4397. DOI: 10.1021/acs.molpharmaceut.7b01137.
- <sup>40</sup> Skalic, M.; Sabbadin, D.; Sattarov, B.; Sciabola, S.; De Fabritiis, G. From Target to Drug: Generative Modeling for the Multimodal Structure-Based Ligand Design. *Molecular Pharmaceutics* **2019**, *16* (10), 4282-4291. DOI: 10.1021/acs.molpharmaceut.9b00634.
- <sup>41</sup> Gómez-Bombarelli, R.; Wei, J. N.; Duvenaud, D.; Hernández-Lobato, J. M.; Sánchez-Lengeling, B.; Sheberla, D.; Aguilera-Iparraguirre, J.; Hirzel, T. D.; Adams, R. P.; Aspuru-Guzik, A. Automatic Chemical Design Using a Data-Driven Continuous Representation of Molecules. *ACS Central Science* **2018**, *4* (2), 268-276. DOI: 10.1021/acscentsci.7b00572.
- <sup>42</sup> Sousa, T.; Correia, J.; Pereira, V.; Rocha, M. Combining Multi-objective Evolutionary Algorithms with Deep Generative Models Towards Focused Molecular Design. Cham, 2021; Springer International Publishing: pp 81-96.
- <sup>43</sup> Chenthamarakshan, V.; Das, P.; Hoffman, S. C.; Strobelt, H.; Padhi, I.; Lim, K. W.; Hoover, B.; Manica, M.; Born, J.; Laino, T.; et al. CogMol: target-specific and selective drug design for COVID-19 using deep generative models. In Proceedings of the 34th International Conference on Neural Information Processing Systems, Vancouver, BC, Canada; 2020.
- <sup>44</sup> Lim, J.; Ryu, S.; Kim, J. W.; Kim, W. Y. Molecular generative model based on conditional variational autoencoder for de novo molecular design. *Journal of Cheminformatics* **2018**, *10* (1), 31. DOI: 10.1186/s13321-018-0286-7.
- <sup>45</sup> Simonovsky, M.; Komodakis, N. GraphVAE: Towards Generation of Small Graphs Using Variational Autoencoders. Cham, 2018; Springer International Publishing: pp 412-422.

- <sup>46</sup> Wang, S.; Song, T.; Zhang, S.; Jiang, M.; Wei, Z.; Li, Z. Molecular substructure tree generative model for de novo drug design. *Briefings in Bioinformatics* **2022**, *23* (2). DOI: 10.1093/bib/bbab592.
- <sup>47</sup> Kang, S.; Cho, K. Conditional Molecular Design with Deep Generative Models. *Journal of Chemical Information and Modeling* **2019**, *59* (1), 43-52. DOI: 10.1021/acs.jcim.8b00263.
- <sup>48</sup> Samanta, B.; De, A.; Jana, G.; Chattaraj, P. K.; Ganguly, N.; Rodriguez, M. G. NeVAE: A Deep Generative Model for Molecular Graphs. *Proceedings of the AAAI Conference on Artificial Intelligence* **2019**, *33* (01), 1110-1117. DOI: 10.1609/aaai.v33i01.33011110 (accessed 2023/08/09).
- <sup>49</sup> Lim, J.; Hwang, S.-Y.; Moon, S.; Kim, S.; Kim, W. Y. Scaffold-based molecular design with a graph generative model. *Chemical Science* **2020**, *11* (4), 1153-1164, 10.1039/C9SC04503A. DOI: 10.1039/C9SC04503A.
- <sup>50</sup> Jin, W.; Barzilay, R.; Jaakkola, T. Junction Tree Variational Autoencoder for Molecular Graph Generation. In Proceedings of the 35th International Conference on Machine Learning, Proceedings of Machine Learning Research; 2018.
- <sup>51</sup> Dollar, O.; Joshi, N.; Beck, D. A. C.; Pfandtner, J. Attention-based generative models for de novo molecular design. *Chemical Science* **2021**, *12* (24), 8362-8372, 10.1039/D1SC01050F. DOI: 10.1039/D1SC01050F.
- <sup>52</sup> Krishnan, S. R.; Bung, N.; Vangala, S. R.; Srinivasan, R.; Bulusu, G.; Roy, A. De Novo Structure-Based Drug Design Using Deep Learning. *Journal of Chemical Information and Modeling* **2022**, *62* (21), 5100-5109. DOI: 10.1021/acs.jcim.1c01319.
- <sup>53</sup> Filella-Merce, I.; Molina, A.; Orzechowski, M.; Díaz, L.; Zhu, Y.; Mor, J.; Malo, L.; Yekkiral, A.; Ray, S.; Guallar, V. Optimizing Drug Design by Merging Generative AI With Active Learning Frameworks. *ArXiv* **2023**, *abs/2305.06334*.
- <sup>54</sup> Zhavoronkov, A.; Ivanenkov, Y. A.; Aliper, A.; Veselov, M. S.; Aladinskiy, V. A.; Aladinskaya, A. V.; Terentiev, V. A.; Polykovskiy, D. A.; Kuznetsov, M. D.; Asadulaev, A.; et al. Deep learning enables rapid identification of potent DDR1 kinase inhibitors. *Nature Biotechnology* **2019**, *37* (9), 1038-1040. DOI: 10.1038/s41587-019-0224-x.
- <sup>55</sup> Abeer, A. N. M. N.; Urban, N. M.; Weil, M. R.; Alexander, F. J.; Yoon, B.-J. Latent Space Optimization of Generative Molecular Design Models. *ArXiv* **2022**, *abs/2203.00526*.
- <sup>56</sup> Nesterov, V.; Wieser, M.; Roth, V. 3DMolNet: A Generative Network for Molecular Structures. *ArXiv* **2020**, *abs/2010.06477*.
- <sup>57</sup> Skalic, M.; Jiménez, J.; Sabbadin, D.; De Fabritiis, G. Shape-Based Generative Modeling for de Novo Drug Design. *Journal of Chemical Information and Modeling* **2019**, *59* (3), 1205-1214. DOI: 10.1021/acs.jcim.8b00706.

- <sup>58</sup> Hong, S. H.; Ryu, S.; Lim, J.; Kim, W. Y. Molecular Generative Model Based on an Adversarially Regularized Autoencoder. *Journal of Chemical Information and Modeling* **2020**, *60* (1), 29-36. DOI: 10.1021/acs.jcim.9b00694.
- <sup>59</sup> Kadurin, A.; Aliper, A.; Kazennov, A.; Mamoshina, P.; Vanhaelen, Q.; Khrabrov, K.; Zhavoronkov, A. The cornucopia of meaningful leads: Applying deep adversarial autoencoders for new molecule development in oncology. *Oncotarget* **2016**, *8* (7).
- <sup>60</sup> Kadurin, A.; Nikolenko, S.; Khrabrov, K.; Aliper, A.; Zhavoronkov, A. druGAN: An Advanced Generative Adversarial Autoencoder Model for de Novo Generation of New Molecules with Desired Molecular Properties in Silico. *Molecular Pharmaceutics* **2017**, *14* (9), 3098-3104. DOI: 10.1021/acs.molpharmaceut.7b00346.
- <sup>61</sup> Polykovskiy, D.; Zhebrak, A.; Vetrov, D.; Ivanenkov, Y.; Aladinskiy, V.; Mamoshina, P.; Bozdaganyan, M.; Aliper, A.; Zhavoronkov, A.; Kadurin, A. Entangled Conditional Adversarial Autoencoder for de Novo Drug Discovery. *Molecular Pharmaceutics* **2018**, *15* (10), 4398-4405. DOI: 10.1021/acs.molpharmaceut.8b00839.
- <sup>62</sup> Mao, J.; Wang, J.; Zeb, A.; Cho, K.-H.; Jin, H.; Kim, J.; Lee, O.; Wang, Y.; No, K. T. Transformer-Based Molecular Generative Model for Antiviral Drug Design. *Journal of Chemical Information and Modeling* **2023**. DOI: 10.1021/acs.jcim.3c00536.
- <sup>63</sup> Wei, L.; Fu, N.; Song, Y.; Wang, Q.; Hu, J. Probabilistic Generative Transformer Language Models for Generative design of Molecules. *ArXiv* **2022**, *abs/2209.09406*.
- <sup>64</sup> Wang, J.; Mao, J.; Wang, M.; Le, X.; Wang, Y. Explore drug-like space with deep generative models. *Methods* **2023**, *210*, 52-59. DOI: <https://doi.org/10.1016/j.ymeth.2023.01.004>.
- <sup>65</sup> Grechishnikova, D. Transformer neural network for protein-specific de novo drug generation as a machine translation problem. *Scientific Reports* **2021**, *11* (1), 321. DOI: 10.1038/s41598-020-79682-4.
- <sup>66</sup> Kim, H.; Na, J.; Lee, W. B. Generative Chemical Transformer: Neural Machine Learning of Molecular Geometric Structures from Chemical Language via Attention. *Journal of Chemical Information and Modeling* **2021**, *61* (12), 5804-5814. DOI: 10.1021/acs.jcim.1c01289.
- <sup>67</sup> Wang, W.; Wang, Y.; Zhao, H.; Sciabola, S. A Transformer-based Generative Model for De Novo Molecular Design. *ArXiv* **2022**, *abs/2210.08749*.
- <sup>68</sup> Chen, Y.; Wang, Z.; Wang, L.; Wang, J.; Li, P.; Cao, D.; Zeng, X.; Ye, X.; Sakurai, T. Deep generative model for drug design from protein target sequence. *Journal of Cheminformatics* **2023**, *15* (1), 38. DOI: 10.1186/s13321-023-00702-2.



- <sup>69</sup> Bagal, V.; Aggarwal, R.; Vinod, P. K.; Priyakumar, U. D. MolGPT: Molecular Generation Using a Transformer-Decoder Model. *Journal of Chemical Information and Modeling* **2022**, *62* (9), 2064-2076. DOI: 10.1021/acs.jcim.1c00600.
- <sup>70</sup> Prykhodko, O.; Johansson, S. V.; Kotsias, P.-C.; Arús-Pous, J.; Bjerrum, E. J.; Engkvist, O.; Chen, H. A de novo molecular generation method using latent vector based generative adversarial network. *Journal of Cheminformatics* **2019**, *11* (1), 74. DOI: 10.1186/s13321-019-0397-9.
- <sup>71</sup> Abbasi, M.; Santos, B. P.; Pereira, T. C.; Sofia, R.; Monteiro, N. R. C.; Simões, C. J. V.; Brito, R. M. M.; Ribeiro, B.; Oliveira, J. L.; Arrais, J. P. Designing optimized drug candidates with Generative Adversarial Network. *Journal of Cheminformatics* **2022**, *14* (1), 40. DOI: 10.1186/s13321-022-00623-6.
- <sup>72</sup> Vaswani, A.; Shazeer, N.; Parmar, N.; Uszkoreit, J.; Jones, L.; Gomez, A. N.; Kaiser, Ł. u.; Polosukhin, I. Attention is All you Need. 2017; Curran Associates, Inc.: Vol. 30.
- <sup>73</sup> Devlin, J.; Chang, M.-W.; Lee, K.; Toutanova, K. BERT: Pre-training of Deep Bidirectional Transformers for Language Understanding. *ArXiv* **2019**, *abs/1810.04805*.
- <sup>74</sup> Weininger, D. SMILES, a chemical language and information system. 1. Introduction to methodology and encoding rules. *Journal of Chemical Information and Computer Sciences* **1988**, *28* (1), 31-36. DOI: 10.1021/ci00057a005.
- <sup>75</sup> Bongini, P.; Bianchini, M.; Scarselli, F. Molecular generative Graph Neural Networks for Drug Discovery. *Neurocomputing* **2021**, *450*, 242-252. DOI: <https://doi.org/10.1016/j.neucom.2021.04.039>.
- <sup>76</sup> Li, Y.; Zhang, L.; Liu, Z. Multi-objective de novo drug design with conditional graph generative model. *Journal of Cheminformatics* **2018**, *10* (1), 33. DOI: 10.1186/s13321-018-0287-6.
- <sup>77</sup> Mercado, R.; Rastemo, T.; Lindelöf, E.; Klambauer, G.; Engkvist, O.; Chen, H.; Bjerrum, E. J. Graph Networks for Molecular Design. *ChemRxiv* **2020**. DOI: 10.26434/chemrxiv.12843137.v1.
- <sup>78</sup> Khemchandani, Y.; O'Hagan, S.; Samanta, S.; Swainston, N.; Roberts, T. J.; Bollegala, D.; Kell, D. B. DeepGraphMolGen, a multi-objective, computational strategy for generating molecules with desirable properties: a graph convolution and reinforcement learning approach. *Journal of Cheminformatics* **2020**, *12* (1), 53. DOI: 10.1186/s13321-020-00454-3.
- <sup>79</sup> You, J.; Liu, B.; Ying, R.; Pande, V.; Leskovec, J. Graph Convolutional Policy Network for Goal-Directed Molecular Graph Generation. *ArXiv* **2018**, *abs/1806.02473*.
- <sup>80</sup> Atance, S. R.; Diez, J. V.; Engkvist, O.; Olsson, S.; Mercado, R. De Novo Drug Design Using Reinforcement Learning with Graph-Based Deep Generative Models. *Journal of Chemical Information and Modeling* **2022**, *62* (20), 4863-4872. DOI: 10.1021/acs.jcim.2c00838.

- <sup>81</sup> Li, Y.; Pei, J.; Lai, L. Structure-based de novo drug design using 3D deep generative models. *Chemical Science* **2021**, *12* (41), 13664-13675, 10.1039/D1SC04444C. DOI: 10.1039/D1SC04444C.
- <sup>82</sup> Seo, S.; Lim, J.; Kim, W. Y. Molecular Generative Model via Retrosynthetically Prepared Chemical Building Block Assembly. *Advanced Science* **2023**, *10* (8), 2206674. DOI: <https://doi.org/10.1002/advs.202206674>.
- <sup>83</sup> Jeon, W.; Kim, D. Autonomous molecule generation using reinforcement learning and docking to develop potential novel inhibitors. *Scientific Reports* **2020**, *10* (1), 22104. DOI: 10.1038/s41598-020-78537-2.
- <sup>84</sup> Simm, G.; Pinsler, R.; Hernandez-Lobato, J. M. Reinforcement Learning for Molecular Design Guided by Quantum Mechanics. In Proceedings of the 37th International Conference on Machine Learning, Proceedings of Machine Learning Research; 2020.
- <sup>85</sup> Horwood, J.; Noutahi, E. Molecular Design in Synthetically Accessible Chemical Space via Deep Reinforcement Learning. *ACS Omega* **2020**, *5* (51), 32984-32994. DOI: 10.1021/acsomega.0c04153.
- <sup>86</sup> Bickerton, G. R.; Paolini, G. V.; Besnard, J.; Muresan, S.; Hopkins, A. L. Quantifying the chemical beauty of drugs. *Nature Chemistry* **2012**, *4* (2), 90-98. DOI: 10.1038/nchem.1243.
- <sup>87</sup> Liu, H.; Li, Z.; Hall, D.; Liang, P.; Ma, T. Sophia: A Scalable Stochastic Second-order Optimizer for Language Model Pre-training. *ArXiv* **2023**, *abs/2305.14342*.
- <sup>88</sup> Mendez, D.; Gaulton, A.; Bento, A. P.; Chambers, J.; De Veij, M.; Félix, E.; Magariños, María P.; Mosquera, Juan F.; Mutowo, P.; Nowotka, M.; et al. ChEMBL: towards direct deposition of bioassay data. *Nucleic Acids Research* **2019**, *47* (D1), D930-D940. DOI: 10.1093/nar/gky1075 (accessed 8/21/2023).
- <sup>89</sup> Brown, N.; Fiscato, M.; Segler, M. H. S.; Vaucher, A. C. Guacamol: Benchmarking Models for de Novo Molecular Design. *Journal of Chemical Information and Modeling* **2019**, *59* (3), 1096-1108. DOI: 10.1021/acs.jcim.8b00839.
- <sup>90</sup> Sterling, T.; Irwin, J. J. ZINC 15 – Ligand Discovery for Everyone. *Journal of Chemical Information and Modeling* **2015**, *55* (11), 2324-2337. DOI: 10.1021/acs.jcim.5b00559.
- <sup>91</sup> Polykovskiy, D.; Zhebrak, A.; Sanchez-Lengeling, B.; Golovanov, S.; Tatanov, O.; Belyaev, S.; Kurbanov, R.; Artamonov, A.; Aladinskiy, V.; Veselov, M.; et al. Molecular Sets (MOSES): A Benchmarking Platform for Molecular Generation Models. *Frontiers in Pharmacology* **2020**, *11*, 565644. DOI: 10.3389/fphar.2020.565644.
- <sup>92</sup> Liu, T.; Lin, Y.; Wen, X.; Jorissen, R. N.; Gilson, M. K. BindingDB: a web-accessible database of experimentally determined protein-ligand binding affinities. *Nucleic Acids Research* **2007**, *35* (Database issue), D198-201. DOI: 10.1093/nar/gkl999.

- <sup>93</sup> RDKit: Open-source cheminformatics. <https://www.rdkit.org>.
- <sup>94</sup> Corso, G.; Stärk, H.; Jing, B.; Barzilay, R.; Jaakkola, T. DiffDock: Diffusion Steps, Twists, and Turns for Molecular Docking. *ArXiv* **2023**, *abs/2210.01776*.
- <sup>95</sup> East, K. W.; Newton, J. C.; Morzan, U. N.; Narkhede, Y. B.; Acharya, A.; Skeens, E.; Jogl, G.; Batista, V. S.; Palermo, G.; Lisi, G. P. Allosteric Motions of the CRISPR–Cas9 HNH Nuclease Probed by NMR and Molecular Dynamics. *Journal of the American Chemical Society* **2020**, *142* (3), 1348-1358. DOI: 10.1021/jacs.9b10521.
- <sup>96</sup> Bouysset, C.; Fiorucci, S. ProLIF: a library to encode molecular interactions as fingerprints. *Journal of Cheminformatics* **2021**, *13* (1), 72. DOI: 10.1186/s13321-021-00548-6.
- <sup>97</sup> Liu, Z.; Su, M.; Han, L.; Liu, J.; Yang, Q.; Li, Y.; Wang, R. Forging the Basis for Developing Protein–Ligand Interaction Scoring Functions. *Accounts of Chemical Research* **2017**, *50* (2), 302-309. DOI: 10.1021/acs.accounts.6b00491.
- <sup>98</sup> Maaten, L. v. d.; Hinton, G. E. Visualizing Data using t-SNE. *Journal of Machine Learning Research* **2008**, *9*, 2579-2605.
- <sup>99</sup> Wang, Y.; Zhao, H.; Sciabola, S.; Wang, W. cMolGPT: A Conditional Generative Pre-Trained Transformer for Target-Specific De Novo Molecular Generation. *Molecules* **2023**, *28* (11). DOI: 10.3390/molecules28114430.